RADAR DETECTABILITY STUDIES OF SLOW AND SMALL ZODIACAL DUST CLOUD PARTICLES. I. THE CASE OF ARECIBO 430 MHz METEOR HEAD ECHO OBSERVATIONS

D. Janches[1], J. M. C. Plane[2], D. Nesvorný[3], W. Feng[2], D. Vokrouhlický[4], and M. J. Nicolls[5]

[1] Space Weather Laboratory, Mail Code 674, GSFC/NASA, Greenbelt, MD 20771, USA; diego.janches@nasa.gov
[2] School of Chemistry, University of Leeds, Leeds LS2 9JT, UK; j.m.c.plane@leeds.ac.uk, w.feng@leeds.ac.uk
[3] SouthWest Research Institute, Boulder, CO 80302, USA; davidn@boulder.swri.edu
[4] Institute of Astronomy, Charles University, Prague, Czech Republic; vokrouhl@cesnet.cz
[5] SRI International, Menlo Park, CA 94025, USA; Michael.Nicolls@sri.com

ABSTRACT

Recent model development of the Zodiacal Dust Cloud (ZDC) argues that the incoming flux of meteoric material into the Earth's upper atmosphere is mostly undetected by radars because they cannot detect small extraterrestrial particles entering the atmosphere at low velocities due to the relatively small production of electrons. In this paper, we present a new methodology utilizing meteor head echo radar observations that aims to constrain the ZDC physical model by ground-based measurements. In particular, for this work, we focus on Arecibo 430 MHz observations since this is the most sensitive radar utilized for this type of observations to date. For this, we integrate and employ existing comprehensive models of meteoroid ablation, ionization, and radar detection to enable accurate interpretation of radar observations and show that reasonable agreement in the hourly rates is found between model predictions and Arecibo observations when (1) we invoke the lower limit of the model predicted flux ($\sim$16 t d^{-1}) and (2) we estimate the ionization probability of ablating metal atoms using laboratory measurements of the ionization cross sections of high-speed metal atom beams, resulting in values up to two orders of magnitude lower than the extensively utilized figure reported by Jones for low-speed meteors. However, even at this lower limit, the model overpredicts the slow portion of the Arecibo radial velocity distributions by a factor of three, suggesting that the model requires some revision.

Key words: atmospheric effects – meteorites, meteors, meteoroids – methods: observational – zodiacal dust

Online-only material: color figures

1. INTRODUCTION

The global meteoric input to the upper atmosphere is a hotly debated quantity, with estimates varying by two orders of magnitude, depending on measuring techniques (Plane 2012). The majority of the input is in the form of microgram-size particles that, in most cases, completely ablate injecting metals to planetary atmospheres. Accurate constraint of this quantity is crucial for a variety of research areas. The meteoric mass input is transported into the middle atmosphere, where the coupling between the lower and upper atmosphere takes place. If the meteoric mass input is closer to the upper limits of current estimates, then the vertical transport in the middle atmosphere must be considerably faster than generally believed; while the opposite case would require the revision of our understanding of dust evolution in the solar system. There is thus a need for better understanding of this quantity in a comprehensive manner, that is, by combining models of dust release from celestial bodies, orbital evolution, ablation, and ionization processes when dust particles encounter planetary atmospheres and ultimately by constraining these models simultaneously by all available observing techniques.

A new Zodiacal Dust Cloud (ZDC) model, hereafter referred as ZoDy, recently developed by Nesvorný et al. (2010), represents a fundamental approach to understanding the origins of interplanetary dust particles (IDPs). The model follows the dynamical evolution of dust particles after ejection, utilizing the orbital properties of comets and asteroids. One of the main results is that it predicts that 85%–95% of IR emission of the zodiacal cloud is due to particles originated from Jupiter Fam-

ily Comets (JFCs), with the remainder from the asteroid belt, Halley-type comets, and Oort Cloud comets (OCCs). Furthermore, the modeled results show that most of the dust, which drifts down toward the inner solar system under the influence of Poynting–Robertson drag, has a mass in the range 1–10 μg and provides a continuous input of extraterrestrial material into Earth that has dynamical characteristics that are in disagreement with various type of measurement results. Specifically, the model predicts that most of the IDPs enter the terrestrial atmosphere from a near-prograde orbit with a mean speed with respect to Earth of about 14 km s^{-1} and a peak at 12 km s^{-1} (solid line in Figure 1). The low average speed and the absence of significant orbital eccentricities, also a prediction of the model, do not accord with various types of meteor radar observations, which record average speeds closer to 30 km s^{-1} (dashed line in Figure 1). Furthermore, these low speeds are in disagreement with results from the impact experiments on board the five *Lunar Orbiters* and *Explorers XVI* and *XXIII* (the latter are the same detectors flown near the Earth (P. Brown 2014, private communication). The impact rate at the moon was around one half that of the Earth to a limiting mass of $>10^{-9}$ g. The factor of roughly two indicates that the speed needs to be approximately (at the top of Earth's atmosphere) $\sim$15 km s^{-1}. For ZoDy-like values (just $\sim$1 km s^{-1} from escape speed, so just 12–13 km s^{-1}), the enhancement between the Earth and Moon would be many times larger (Zook 1975). More recently, Cremonese et al. (2013) showed that in order to model the Na production on the Moon by micrometeoroid impacts with masses in the similar range than those considered by ZoDy, the mean velocity of the impactors was required to be 15.3 km s^{-1}
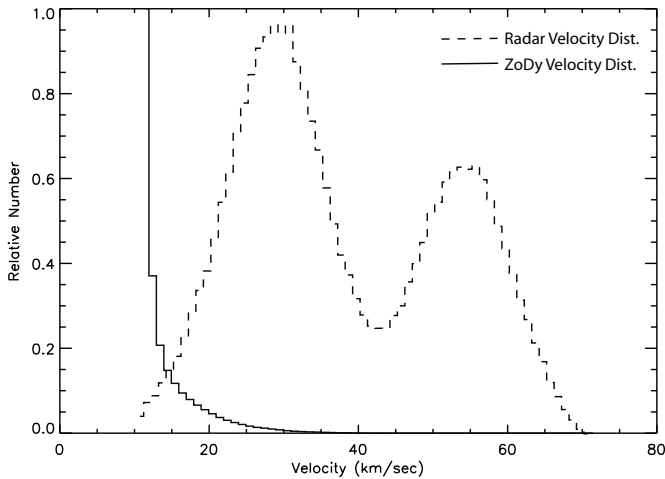
Figure 1. Solid line shows the velocity distribution resulting from ZoDy (Nesvorný et al. 2010). The dashed line represents the velocity distribution at the top of the atmosphere generally measured by radars (Fentzke & Janches 2008).

and $18.6 \ \mathrm{km \, s^{-1}}$ at the Moon and Earth, respectively, which is closer to that assumed in the interpretation of the long-duration exposure facility results Love & Brownlee (1993).

ZoDy is currently quantitatively only constrained by *Infrared Astronomical Satellite* (*IRAS*) observations of the ZDC and originally predicted a total global meteor mass input onto the Earth's atmosphere equal to $270 \ \mathrm{t \, d^{-1}}$ (metric tons). However, Nesvorný et al. (2011a) later improved ZoDy by including a perihelion distance (q) dependent meteoroid production rate, taking into account orbits with $q < 1.5$ AU, a continuous size frequency distribution of particles instead of the original delta functions, and the proper inclusion of collisional lifetimes of JFC particles, which resulted in a more precise parameterization of their collisional disruption in space. These improvements resulted in a revised total mass input on Earth of $32 \ \mathrm{t \, d^{-1}}$. Because the *IRAS* observations primarily constrain the modeled ZDC cross section and not the mass, then different assumptions regarding the particle mass distribution or distributions of q result in the uncertainties on the total flux being as large as 50% (Nesvorný et al. 2011a), where the cross section is given by

$$\sigma_{\mathrm{ZoDy}} = \int \pi r^2 N(r) dr, \qquad (1)$$

where πr^2 is the cross section of a particle with radius r and $N(r)$ is the total number of particles with radius r contributing to the IR emission. This total cross section determines the ability of ZoDy to emit in infrared, and thus to be constrained from observations.

In addition to a revision to the model, Nesvorný et al. (2011a) attempted to loosely constrain the model with terrestrial observations using results from the Canadian Meteor Orbit Radar (CMOR; Webster et al. 2004) and the Advanced Meteor Orbit Radar (AMOR; Baggaley et al. 1994). The authors concluded that this flux, and consequently most of the incoming meteoric mass flux into the Earth's atmosphere, is mostly undetected by CMOR while the more sensitive AMOR should detect between 10%–50% of the incoming flux predicted by ZoDy, depending on model assumptions. The large difference in detections by specular trail meteor radars, as compared to those from satellite dust impact detector measurements, has been noted in the past by Hughes (1978), who concluded that, similarly

to Nesvorný et al. (2011a), meteor radars cannot be used to retrieve the mass flux reliably. The radar measurements used by Nesvorný et al. (2011a), however, do not have the sensitivity to observe the particle masses dominant in ZoDy when the particles travel at low speeds (because of a low production of electrons through ablating elements making hyperthermal collisions with air molecules). AMOR is the more sensitive of the two meteor radars with reported limiting masses for particles traveling at $30 \ \mathrm{km \, s^{-1}}$ of the order of $1 \ \mu \mathrm{g}$, while CMOR's limiting mass at this speed is two orders of magnitude larger (Galligan & Baggaley 2005; Brown et al. 2008). Therefore, the conclusions reported by Nesvorný et al. (2010, 2011a) that these radars cannot detect most of the ZoDy meteors is consistent with expectations. However, one of ZoDy's main implications that most of this flux comes into the atmosphere largely undetected by ground-based instrumentation could not be unequivocally tested.

It is crucial to constrain the ZDC model with radar observations not only to obtain a unique value of the total incoming mass flux, which must be independent of the observing technique, but also to precisely characterize the orbital distribution of dust in the near-Earth space. The ZDC is the source of meteoroids originating from the so-called sporadic meteor complex (SMC). Ground-based meteor observations with radars detect thousand of sporadic events every day, providing data sets with great statistics optimal to study the ZDC. The SMC is composed of six main directional enhancements of the meteor radiants (i.e., orbital families). These are referred to as apparent sources since they are not linked to their original parent body. These apparent sources are known as the north and south apex, composed mainly of dust from long-period comets and initially studied by Sekanina (1976); the helion and anti-helion, composed of dust from short-period comets originally reported by Hawkins (1956)[6] and Weiss & Smith (1960) and the north and south toroidal composed of dust from Halley-family comets (Jones & Brown 1993; Taylor 1997; Taylor & Elford 1998; Campbell-Brown & Wiegert 2009; Pokorný et al. 2014). Each of these sources produce specific signatures in the radar detected distributions that depend on geographical location of the observer, seasonality, and radar system characteristics (Janches & Chau 2005; Janches et al. 2006; Fentzke & Janches 2008; Fentzke et al. 2009; Sparks et al. 2009; Sparks & Janches 2009a, 2009b; Pifko et al. 2013). Because of the wide variety of radar systems utilized for meteor observations (Janches et al. 2008, 2014) and their different locations, these observations are key to constraining not only the total amount of meteoric material coming into the atmosphere, but also the directionality and seasonality of the flux, which are directly related to the orbital characteristics.

The most sensitive radar in the world currently used for meteor studies is the Arecibo 430 MHz radar. While traditional very high frequency (VHF) meteor radars (often called all-sky radars) such as CMOR and AMOR primarily detect the specular reflection of meteor trails traveling perpendicular to the line of sight of the scattering trail, high-power and large-aperture (HPLA) radars, such as Arecibo, efficiently detect meteor head echoes (Janches et al. 2003, 2014). Trails are generally semi-stationary echoes that originate from the ionization left behind by the meteoroid (Baggaley 2002) and are confined to one altitude. Head echoes, on the other hand, are reflections from the plasma immediately surrounding the meteoroid itself traveling

---

6 In ZoDy, the main contributions are meteors from those sources (Nesvorný et al. 2010).

at, or near, its speed (Janches et al. 2000a, 2003). HPLA radars are also very sensitive instruments with generally very narrow beam width and much higher transmitted power densities (Janches et al. 2008, 2014) and thus sensitive to the detection of meteors produced by smaller particles because they require a lower amount of electrons than systems like AMOR and CMOR. In this manuscript, we utilize a combination of several models as well as Arecibo meteor observations to determine if the sensitivity of this system is sufficient to constrain ZoDy with ground-based observations. To accomplish this task we (1) determine if Arecibo can detect $1\text{–}10\,\mu$g particles traveling at $11\text{–}20\,\mathrm{km\,s^{-1}}$; and (2) if that is the case, then estimate what portion of the Arecibo meteor observations can be modeled with the flux predicted by ZoDy in order to further constrain the model with ground-based observations.

2. RADAR DETECTION SENSITIVITY MODELING

2.1. Meteor Head Echo Signal-to-noise Ratio

The first task we address is to assess the ability of the Arecibo 430 MHz radar to detect small particles ($m < 10\,\mu$g) traveling at slow velocities ($V < 20\,\mathrm{km\,s^{-1}}$). Although similar attempts have been made in the past (e.g., Janches et al. 2008, 2014), in the work presented here we introduce several improvements to our methodology that include our latest understanding of meteor ablation processes and the determination of the meteor head echo signal-to-noise ratio (S/N) that will be detected by the Arecibo 430 MHz, given a set of meteor dynamical parameters (i.e., mass, velocity, and entry angle). For this we utilize the radar equation given by

$$\mathrm{S/N} = \frac{P_t \lambda_R^2 G^2 \sigma}{(4\pi)^3 P_n R^4}, \qquad (2)$$

where in particular for the observational results we utilize here, P_t is the transmitted power (1 MW), λ_R is the radar wavelength (69 cm), G is one-way antenna gain pattern, R is the meteor range, σ is the meteor radar cross section (RCS), and P_n is the system noise power given by

$$P_n = kT_{\mathrm{sys}}B, \qquad (3)$$

where k is the Boltzmann constant, B is the noise bandwidth (1 MHz), and T_{sys} is the system temperature ($\sim$120 K).

In previous works we have utilized σ as a proxy of the sensitivity of the radar to the detection of meteor head echoes (Janches et al. 2008; Fentzke & Janches 2008; Fentzke et al. 2009; Pifko et al. 2013), which requires the assumption that the antenna radiation pattern is uniform and thus for a particle with a given σ, the resulting S/N will be independent of where the meteor is detected within the radar beam. In the present study we improve our previous treatment by modeling the meteor S/N, a task that requires understanding the relation between Equation (2) and the meteor entry parameters. In other words, we need to calculate how the S/N varies as a function of particle mass, velocity, and entry angle while considering all possible paths that the meteoroid trajectory can take while crossing the radar beam. For this we need to model both the Arecibo antenna gain and σ.

2.2. Arecibo Radar Gain

In order to model the gain (G) of the Arecibo antenna we adopt the same approach reported by Dyrud & Janches (2008),

which characterizes the pattern of the radar main beam as a Gaussian with a 3 dB point at approximately 150 m from the center. The peak of the main lobe is given by

$$G = 10 \times \log_{10}\left(\frac{4\pi A_{\mathrm{eff}}}{\lambda_R^2}\right), \qquad (4)$$

where the A_{eff} is the approximate aperture given by

$$A_{\mathrm{eff}} = \eta \pi 150^2, \qquad (5)$$

where η is the approximate aperture efficiency of 0.7 and 150 m is the Arecibo dish radius, resulting in $G \sim 61$ dB. This is 2 dB lower than considered previously in Janches et al. (2014) because in that work we considered η to be equal to 1. However, this difference is within the expected uncertainty. We also consider the Arecibo first side lobe in which detection occurs frequently (Janches et al. 2004), assuming it to be also a Gaussian centered about 500 m from the center of the main beam and a 3 dB width of 50 m. Although the description of the Arecibo beam as two Gaussians is somewhat simplistic, it is in good agreement with more robust modeling of the antenna pattern described in the past (Breakall & Mathews 1982; Mathews et al. 1997). The peak of the side lobe is considered to be 17 dB lower than the peak of the main beam. This description resulted in good agreements with observations in previous modeling work of head echoes (Dyrud & Janches 2008). It is worth noting that the expected error in the S/N values resulting from Equation (2) introduced by errors in the measured variables of Equations (3) and (4) is approximately 3 dB (factor of two).

2.3. Meteor Radar Cross Section Derived from the Chemical Ablation Model (CABMOD)

The meteoroid RCS depends on the production of electrons as the meteoroid ablates while entering the Earth's atmosphere. In this work, we adopt the description of the RCS reported by Mathews et al. (1997), which assumes that the radar return originates from coherent electron-scatter from the free electrons in the small volume surrounding the meteor and that the backscatter cross section of an ensemble of N_e electrons is given by

$$\sigma(V, \alpha, m) = 4\pi N_e(V, \alpha, m)^2 r_e^2, \qquad (6)$$

where r_e is the classical electron radius ($2.8179402894 \times 10^{-15}$ m) and V, α, and m are the meteoroid entry velocity, zenith angle, and mass, respectively. In this scenario all electrons (single) scatter in-phase and thus the scattered electric fields add so that scattered power is a function of N_e^2. This is valid because the characteristic size of the ensemble is small compared with the radar wavelength (Mathews et al. 1997). We assume also that, at a given time, the diameter of the cloud of electrons producing the head echo is of the order of the atmospheric mean free path (MFP), which is in agreement to various head echo models (Close et al. 2002, 2004), given by

$$\mathrm{MFP}(h) = \frac{R \times T_a(h)}{\sqrt{2}\pi \times d_a^2 \times L \times P_a(h)}, \qquad (7)$$

where R is the gas law constant (8.314510 J (K mol)$^{-1}$), $T_a(h)$ is the atmospheric temperature at a given altitude, d_a is the air molecule collisional cross section (3.57×10^{-10} m), and $P_a(h)$ is the air pressure at a given altitude.

The production rate of electrons depends on the ionization probability β_{ip} (Jones 1997), which in turns depends only on meteoroid mass, composition, and velocity. Radar detectability of meteors has typically been estimated by using a crude average of this parameter (Close et al. 2002, 2005); in reality it can vary up to two orders of magnitude depending on the constituent under consideration (Vondrak et al. 2008). Thus, in order to overcome this limitation we further improve our radar detection sensitivity treatment by including results from the chemical ablation model (CABMOD) developed by Vondrak et al. (2008). CABMOD predicts differential ablation, i.e., the most volatile elements—Na and K—ablate first, followed by the main constituents Fe, Mg, and Si, and finally the most refractory elements such as Ca. The model considers the full treatment of the ablation and ionization of the individual chemical elements by including the following processes: sputtering by inelastic collisions with air molecules before the meteoroids melt; evaporation of atoms and oxides from the molten particle; diffusion-controlled migration of the volatile constituents (Na and K) through the molten particle; and impact ionization of the ablated fragments by hyperthermal collisions with the air molecules. Evaporation is based on thermodynamic equilibrium in the molten meteoroid (treated as a melt of metal oxides), and between the particle and surrounding vapor phase. The loss rate of each element is then estimated by applying Langmuir evaporation. Figure 2 illustrates the elemental injection profiles calculated by CABMOD for two different meteoroid speeds assuming the initial composition of the meteoroids is chondritic (Plane 1991). The two cases shown in this figure in particular have been validated against meteor head echo observations using the Arecibo radar in which the predicted small-scale temporal and spatial features have been observed (Janches et al. 2009).

As shown in Figure 2 the entire ablation profile, and thus electron production, of a meteoroid with a given mass, entry angle, and velocity will occur over a prolonged altitude range (>60 km). However, only a relatively small part of the ablation curve of the meteoroid will occur within the same region of space that is being illuminated by a given radar. If we define the beam entry point (BEP) as the meteoroid altitude when the particle is at a predefined horizontal distance Δx from the beam center, then for meteoroid BEPs higher than a certain value, the particle will cross the radar beam at the beginning of the ablation process when N_e is small and the detected S/N will be below the radar detection threshold. On the other hand, if the BEP is in the range of typical meteor observe altitudes (∼80–120 km; Janches & ReVelle 2005; Sparks & Janches 2009a, 2009b), then the meteoroid will cross the beam during the time when most of the ablation occurs and result in an S/N well above the noise threshold and the event will be detected. Finally, if the BEP is lower than a certain value, most of the ablation of the particle would have occurred before it entered the radar beam and thus the electron production will be low, resulting in an undetected event. This is shown in Figure 3 where three examples of beam entry cases of a given meteor trajectory are displayed. In fact, within this altitude range, there are two different ablation regimes that can produce the detected signal as shown in Janches et al. (2009). The first one occurs at higher altitudes over a narrow altitude range producing very strong signals due to the rapid ablation of the meteoroid alkalis (Na and K), while the second regime produces lower signal intensity at lower altitudes and over a wider range and is produced by the ablation of the main

elements. This effect will be discussed in more detail later in this section.

For the purpose of this work, we use CABMOD to produce look-up tables of elemental injection profiles as well as the number of electrons per unit length along the meteor trajectory as a function of altitude (gray line in Figure 2) for meteoroids of specified mass, speed, and entry angle. The electron density is then multiplied by the MFP at the given altitude in order to obtain N_e. These results are then used in Equation (6), which together with G, is then used in Equation (2) to determine the S/N as a function of (V, α, m) for all possible BEPs. Given the results of ZoDy mentioned in Section 1, we first focused on determining Arecibo's ability to detect $10\,\mu g$ particles traveling at $11\,km\,s^{-1}$. For this purpose we calculate the S/N along the trajectory of the meteor as it crosses the radar beam for BEPs ranging from 80 to 150 km, calculated every 100 m. If at some point along the trajectory the calculated S/N reaches a value above a predefined threshold, we assume that the meteor was detected. The threshold value is determined from Figure 4 where the distribution of detected S/N is shown for nearly 50,000 particles detected during a year-long observing campaign carried out in 2002 utilizing the Arecibo radar. The meteor head echo arises from the radar return scattered back from a plasma region that moves at the speed of the meteoroid. From the measurements the S/N is calculated as

$$\mathrm{S/N} = \frac{\mathrm{Signal} - \mathrm{Noise}}{\mathrm{Noise}}, \qquad (8)$$

where the signal is the intensity of the radar return when the meteor is present and the noise is the intensity of the radar return from the background noise. Typical meteor head echo observations transmit radar pulses approximately every millisecond and since a meteor will take longer time to travel through the radar beam, this technique enables to measure the instantaneous meteor S/N along its trajectory, as long as enough electrons are produced. The details of these measurements have been reported in several investigations employing various radars. Some examples can be found in Janches et al. (2003, 2014); Chau & Woodman (2004); Sparks et al. (2009), and Pifko et al. (2013).

Figure 4 demonstrates the large dynamic range in S/N of the Arecibo detections with a clear peak in the distribution located approximately at 5–6 dB. However, targets with a S/N as low as −30 dB are detected by the radar. In particular, 0.1% of the detections have recorded S/N of −10 dB and approximately one order of magnitude less for S/N values equal to −20 dB. These are significant percentages considering that only 10% of the detected meteors have S/Ns equal to the peak value. Note that although an S/N value of −10 or −20 dB may appear to be low, this value refers to an S/N measurement for a single pulse, in which not only the object is detected but the instantaneous Doppler shift due to its radial velocity can be obtained.

Results from our new methodology are shown in Figure 5, where the three rows represent particles entering at three different zenith angles ($20°$, $40°$, and $60°$). If we define Δx to be equal to 700 m from the radar beam center, which represents the outer edge of the first radar-side lobe (Mathews et al. 1997; Janches et al. 2004; Dyrud & Janches 2008), the three panels on the left of Figure 5 show the meteoroid S/N as a function of altitude for those meteors for which the BEP was such that their S/N exceeded the threshold value at some point during the ablation of the particle while entering the atmosphere (−20 dB for the examples shown in this figure).
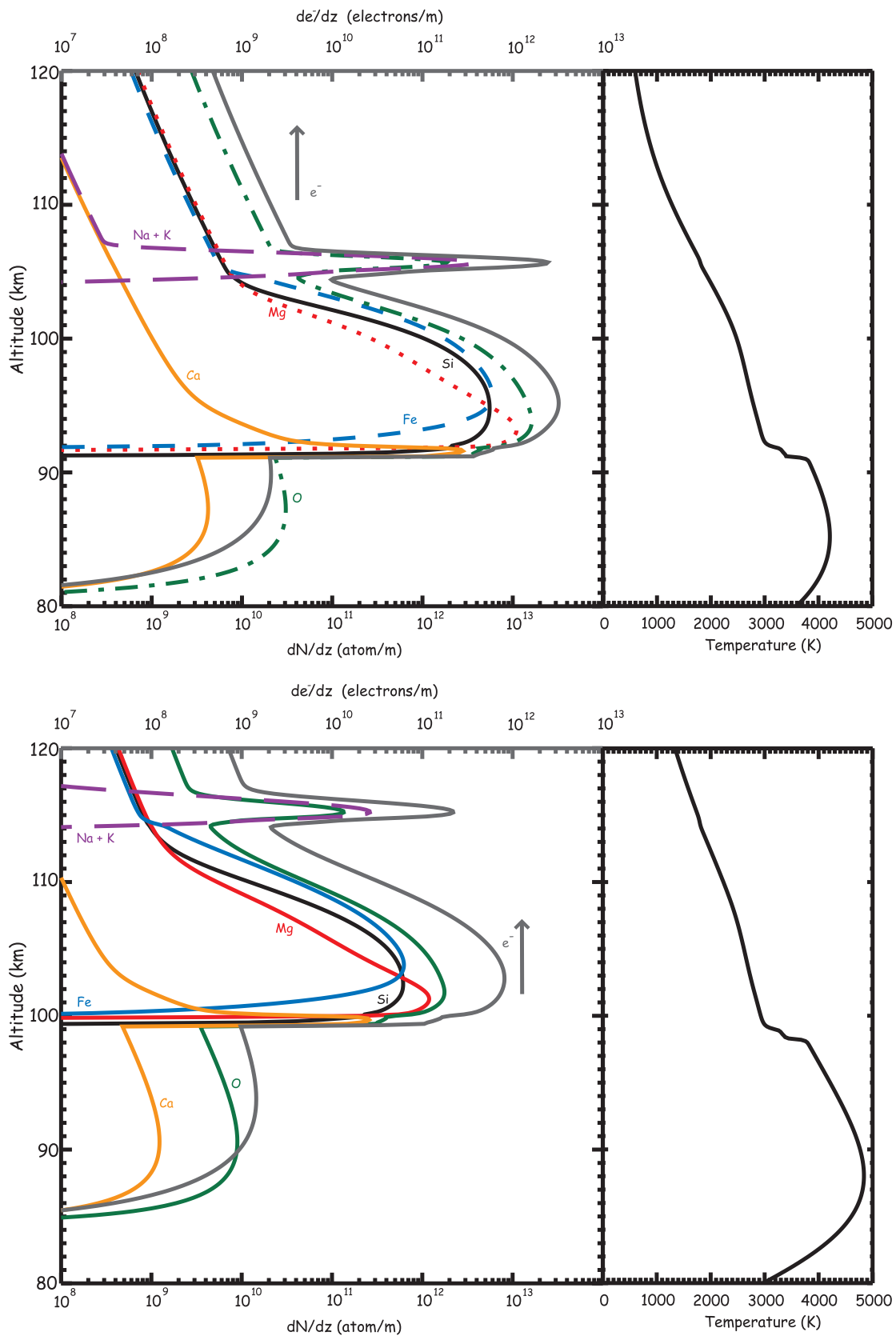
Figure 2. Ablation profiles of the individual elements, electron production, and the meteoroid temperature, for particles moving at 35 (top) and 50 km s^{-1} (bottom) produced by CABMOD. The arrows point at the upper abscissa for the units of the electron profile curve (gray line).

(A color version of this figure is available in the online journal.)
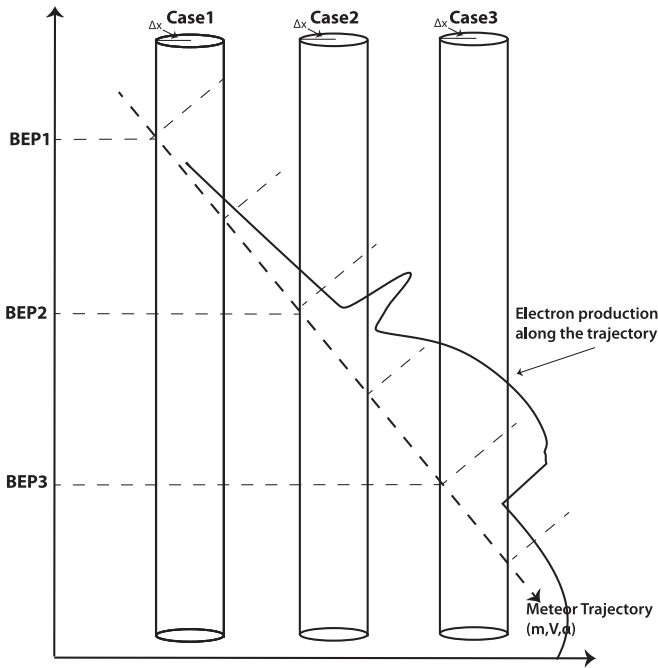
Figure 3. Three possible entry points to the Arecibo radar beam by a given meteor.

Figure 4. Distribution of measured meteor head echo S/N (in percent of total) for all the meteors detected by the Arecibo Observatory during the 2002 campaign. The dash lines indicate that over 0.1% of the detected meteors will have S/N above -10 dB and approximately one and two orders of magnitude lower percentages for S/N values of -20 and -30, respectively.

That is, particles with higher or lower BEPs would have resulted in meteors with undetected S/Ns because significant ablation would have occurred before or after crossing the radar beam. For reference purposes, we also show in these panels vertical lines representing Arecibo detection threshold of -30, -20, and -10 dB. The three panels on the right side of Figure 5 show the meteoroid trajectories (traveled altitude versus traveled horizontal distance; dash lines). The solid blue portion of the trajectories show the section during which the meteor was detectable (i.e., the S/N value was above the detectable threshold). Plotted on these panels is also G in dB (left vertical axis) to provide an indication of where in the radar beam these meteors become detectable.

The results shown in Figure 5 assumes that all these trajectories will cross the radar beam at the center (maximum gain). This is represented in Figure 6, where a horizontal cross section of the radar main beam and first side lobe is shown. The dash lines represent the cases considered in this work, that is, meteors crossing the center and traveling through the 3 dB point (150 m off center). Figure 7 shows the same cases but assuming that the trajectory crosses the beam at the 3 dB point (Figure 6). Examining Figures 5 and 7, we can conclude that, according to our model, a 10 μg particle traveling at 11 km s^{-1} will produce enough electrons and thus an echo radar return signal to be detectable by the Arecibo radar. However, this is true as long as the value of the meteor BEP falls within a certain range of altitudes, which for this case is very narrow, as can be seen in these figures. In addition, it is observed that the range of BEPs for which detectable S/N will be produced will depend on the entry angle and for the cases displayed in this panel the range is greatest for an entry angle around $40°$ and decreases at both larger and smaller angles. Furthermore, results not shown here indicate that for this particle mass and velocity the head echo S/N will be below the detectable level for entry zenith angles higher than $60°$. This is due to the fact that particles entering at very large zenith angle never heat up enough to melt because the
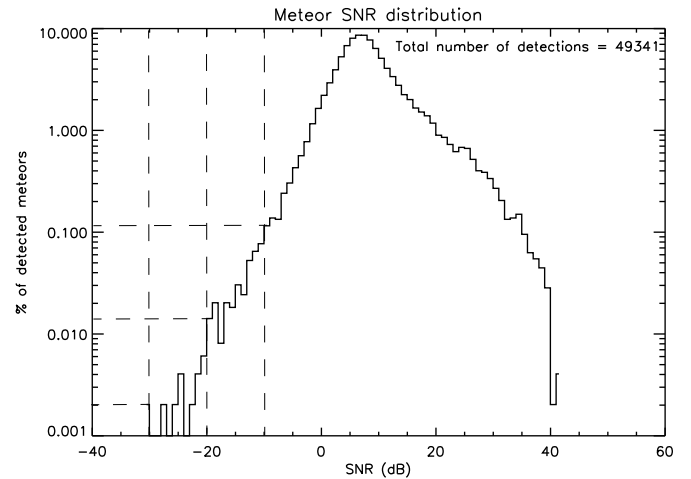
effective scale height experienced by the meteoroid upon entry is inversely proportional to the cosine of the entry zenith angle. This means that the rate of pressure increase encountered by the particle is relatively slow, allowing the particle to radiate heat and stay cool enough to avoid melting. This is in agreement with previous modeling efforts reported by Janches & Chau (2005), Janches et al. (2006), and Fentzke & Janches (2008), who required the assumption of an empirical atmospheric filtering effect, introduced to take into account how the meteor detection rate from a source region varies with elevation above the radar site local horizon. The authors assumed that, on average, meteors with radiant elevations below $20°$ (i.e., entry zenith angles greater than $70°$) should be completely neglected.[7] Our modeling results show that the effective angle at which this filtering effect will occur will depend on the physical properties of the meteoroids (i.e., velocity, composition, and mass) and will be discussed in more detail in the next section.

Figures 8 and 9 show the importance of considering an accurate description of the ablation process that includes the dependence of the ionization efficiency as a function, not only of meteor entry parameters, but also its constituents rather than a crude mean value. Specifically, at low velocities the entry conditions become more limited as the particle mass decreases. For example, Figure 8 shows that a 5 μg traveling at 11 km s^{-1} and with a zenith entry angle of $45°$ will also be detectable by Arecibo as long as the BEP is within a $\sim$0.5 km altitude range. Note that the electron production is completely due to the ablation of alkalis. The transition from becoming undetectable occurs very rapidly as a particle of mass equal to 4 μg entering at the same angle results in an S/N value below the -20 dB Arecibo threshold. Interestingly, this more comprehensive detection treatment that includes the Arecibo radar gain, the meteor S/N, and CABMOD shows good agreement with previously modeled results by our more simplistic approach that considered only the meteor RCS (Fentzke & Janches 2008; Pifko et al. 2013; Janches et al. 2014),

---

[7] Observationally, the effect is evident in the interferometric observations of meteor head echoes result using the Middle and Upper (MU) atmosphere radar in Japan reported by Pifko et al. (2013) and the Southern Argentina Agile Meteor Radar reported by Janches et al. (2014). However, Kero et al. (2012) using similar observations with the MU radar argues that such an effect is not evident in their results.
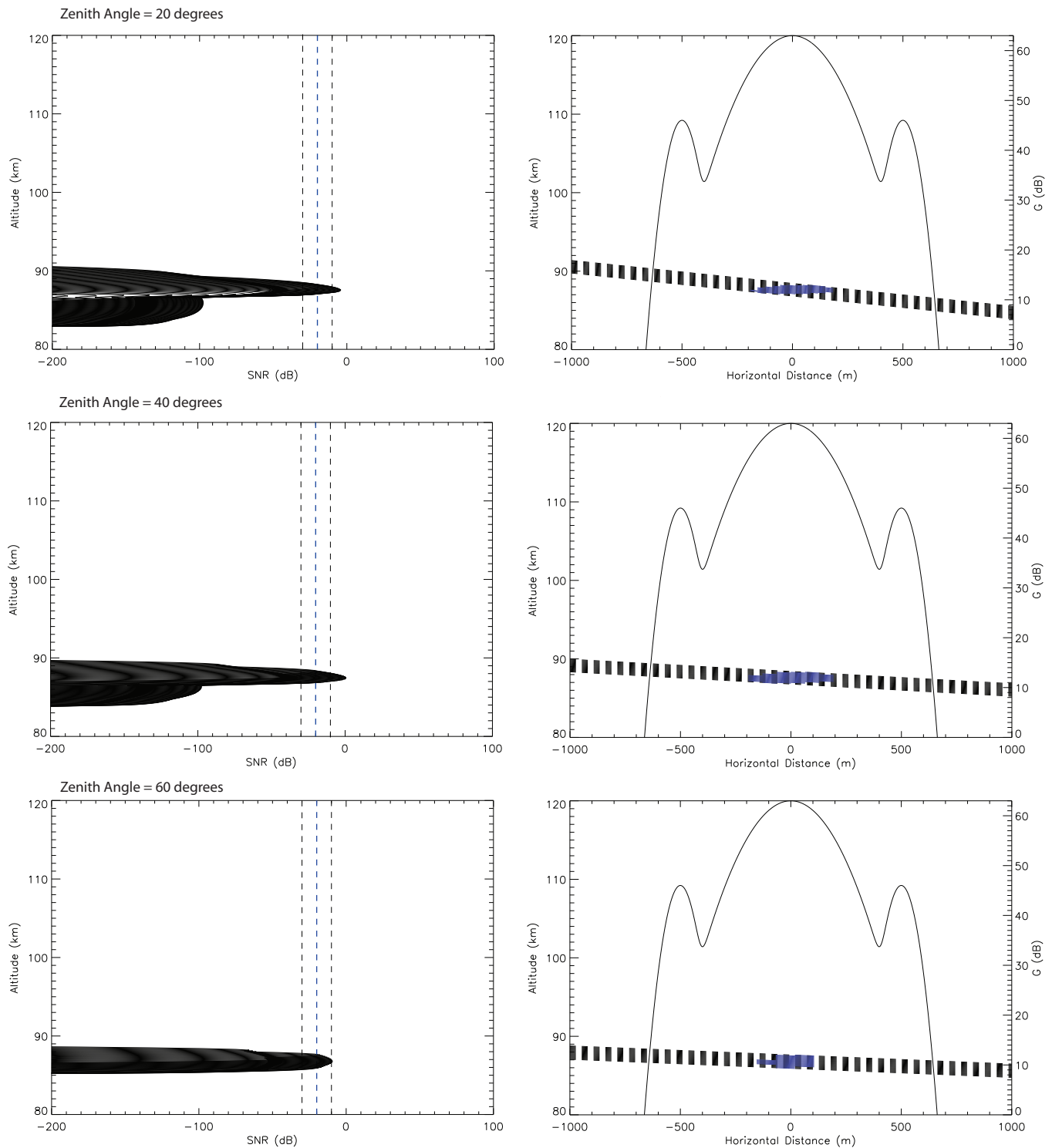
Figure 5. Results for the case of a 10 μg object with a speed of 11 km s^{-1} for three different entry angles. Left panels: meteor S/N as a function of altitude for all BEP for which the meteor calculated S/N was above −20 dB at some point during its trajectory. The vertical lines in these panels represent −30, −20, and −10 dB S/N. Right panels: trajectories (traveled altitude vs. traveled horizontal distance; dash lines) of those meteors for which their S/N exceeded −20 dB at some point during their ablation profile. The solid blue dark portion of the trajectories represents the section during which the S/N was greater than −20 dB. Also plotted on these panels is G in dB (right vertical axis) to provide an indication of where in the radar beam these meteors become detectable. Each row represents a particular zenith entry angle and the trajectories are assume to cross the radar beam center.

(A color version of this figure is available in the online journal.)

which predicted that particles traveling at 15 km s^{-1} would be detected only for masses equal or larger than 1 μg.

On the other hand, Figure 9 shows that with a change of 1 km s^{-1} in the incoming particle velocity the portion of the ablation profile produced by the main elements becomes detectable,

significantly increasing the beam entry conditions required for the resulting meteor to be detected. Because the evaporation rates depend exponentially on the temperature (according to the Herz–Knudsen treatment utilized in CABMOD), the effect will be an apparently sudden change. This is shown in the four
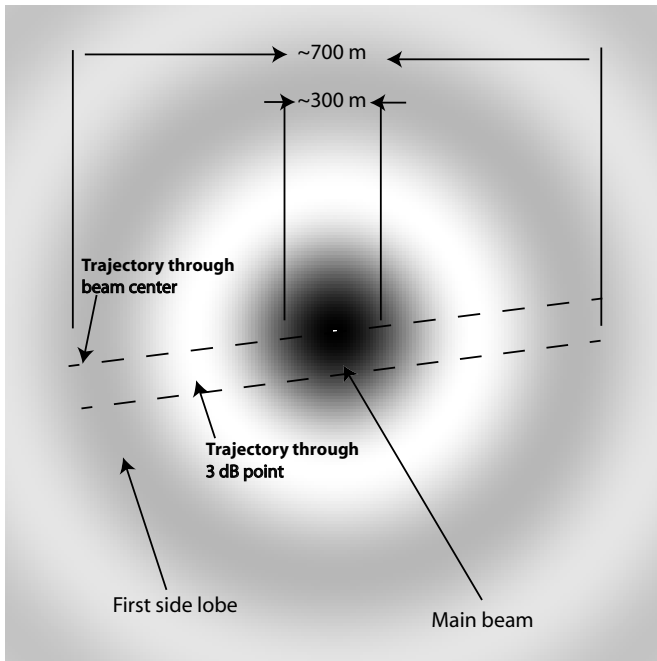
Figure 6. Schematics of two tested meteor trajectories through the radar beam.

panels in Figure 9 where the S/N and trajectories for a $10\,\mu\text{g}$ particle with speeds of 14 and 15 km s^{-1} are displayed for a particle crossing the beam center. Comparing the top two panels of Figure 9, we can observe that the peak of the portion of the ablation curve, which is produced by the evaporation of the main elements increases over 10 dB (i.e., an order of magnitude) in signal strength with only 1 km s^{-1} increase in velocity. The alkalis, on the other hand, ablated efficiently at both speeds and produced enough electrons to enable detection even at the much lower gain side lobes. Furthermore, the figure suggests that if the particle's composition would lack alkali elements at the moment it encounters the atmosphere, then it would have been completely undetected for velocities lower than 14 km s^{-1}. It is important to note that the meteoroid speeds and masses used in these examples are the typical values of the majority of meteoroids predicted by ZoDy, suggesting that Arecibo should detect at least a portion of the flux predicted by ZoDy. It is also worth noticing that if we instead take a more conservative detection threshold of -10 dB, some of the cases discussed would be undetected by the Arecibo radar. For example, this is the case for the a $10\,\mu\text{g}$ particle traveling at a speed of 11 km s^{-1} entering the beam at $60°$ off zenith and passing through the center of the beam (Figure 5; bottom panels) or entering at angles greater than $40°$ for the case of particles traveling off center (Figure 7; middle and bottom panels).

The results presented in Figures 5 and 7–9 show once again that in fact, the Arecibo 430 MHz radar is sensitive to the detection of small/slow meteors and thus the optimal radar to constrain ZoDy with ground-based observations. However, these results also imply that in order to accurately model the ability of a system to detect a certain population of particles, it is not only crucial to understand if the population posses the physical characteristics required to produce enough electrons, but also the probability that a particle from this population with those characteristics will enter the radar beam within the adequate BEP in order for those electrons to produce a detectable signal. In the next section we develop a scheme to estimate

this probability as well as to determine the amount of detected particles given an incoming flux.

3. PROBABILISTIC APPROACH TO ESTIMATE THE RADAR DETECTION EFFICIENCY

In the previous section, we showed that given the β_{ip} values reported by Jones (1997), the Arecibo Observatory can detect meteors produced by particles with mass equal to $10\,\mu\text{g}$ (and smaller) traveling at 11 km s^{-1}. At these low velocities, CABMOD predicts that the particle temperature will not reach values high enough to ablate the main meteoroids elements, such as Fe, Mg, or Si, and thus only the ablation of alkalis (Na and K) will produce electrons (Vondrak et al. 2008). This will occur very rapidly and in a very limited altitude range (see Figures 5 and 7–9; Janches et al. 2009). Since the detection of particles depends on where in the radar beam these electrons are produced, and given the fact that this detection region will become more constrained as the amount of electrons decreases (i.e., with decreasing mass and/or velocity), this implies that the probability of detection will also decrease. On the other hand, we have also shown that only a relatively small increase in the particle's entry velocity is sufficient to "turn on" the ablation of the main elements and "relax" the radar entry constraint. As such, this will add a bias to the observations and the resulting velocity distributions that needs to be corrected for. In the past, this bias was estimated using methods developed for specular trail echo observations using crude averages of the ionization efficiency and other effects typical of a semi-stationary relatively large region of ions and electrons, which resulted in underestimation of the detectability (Hunt et al. 2004; Close et al. 2007; Janches et al. 2008). In this section we introduce a probabilistic approach to estimate this bias by utilizing for the first time a comprehensive model of the meteoroid ablation and by quantifying the spatial limits in which the electron production is optimal for detection.

Our approach is summarized in Figure 10, where a sketch of a flux of particles (F) with a given m and V and originating from a particular radiant characterized by the ecliptic longitude (λ) and ecliptic latitude (β) is impinging the radar illuminated volume in the atmosphere. At a given instantaneous time during the day and season, the ecliptic pair (λ, β) will be located at an angle $\alpha(t)$ with respect to the local zenith, where t denotes the dependance of this quantity at the instantaneous time that it is measured. Furthermore, if we denote as H the altitude range where the atmosphere is dense enough to produce ablation, and hence meteors, independently of their detection, then the projection of the radar volume within this altitude range onto the direction of the flux is represented by the area A_1 and given by

$$A_1(\alpha) = \pi \times \Delta x^2 \times \cos\alpha + \Delta x \times H \times \sin\alpha. \quad (9)$$

As shown in Section 2.3, for a given m, V, and α, out of all the particles that travel through A_1, only those entering the beam between BEP_1 and BEP_2 will produce enough signal for detection, setting a condition that constrains the portion of the incoming flux that will be detected by the radar under consideration. That is, only those meteoroids traveling through the elliptical area identified as A_2 in Figure 10 will be detected by the radar. In order to calculate this area, we define two distances, displayed in Figure 11: (1) the vertical range ($R_v(m, V, \alpha)$) of BEPs for which a detectable signal will be produced and (2) the combined total horizontal distance ($R_h(m, V, \alpha)$) during which a detectable signal is produced. Once they are obtained,
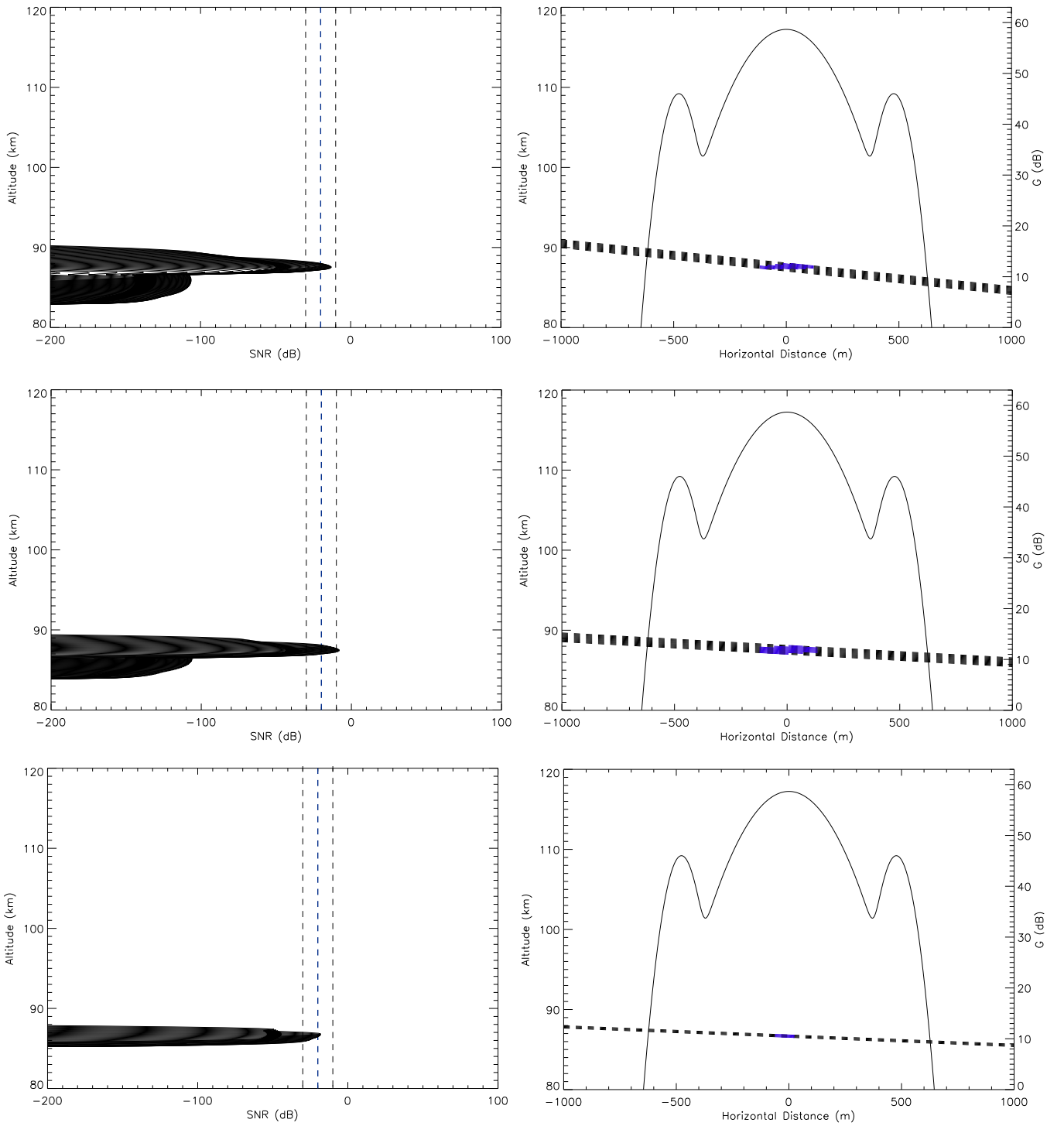
Figure 7. Same as Figure 5 but for trajectories crossing the 3 dB point of the radar beam (i.e., 150 m off center).
(A color version of this figure is available in the online journal.)

we define A_2 as

$$A_2(m, V, \alpha) = \pi \times \left(\frac{R_h(m, V, \alpha)}{2} \right)^2 \times \cos \alpha + \pi$$
$$\times \frac{R_h(m, V, \alpha) \times R_v(m, V, \alpha)}{4} \times \sin \alpha.$$
$$(10)$$

Note that A_1 is only dependent on the zenith angle while A_2 depends on the particle's characteristics. Given these two areas,

we can define the probability of detection of a particle with a given mass, velocity, and entry angle as

$$P(V, \alpha, m) = \frac{A_2(V, \alpha, m)}{A_1(\alpha)}. \qquad (11)$$

In this work we define H as the total range of altitudes in which meteors are observed at Arecibo. This value is obtained from the observed altitude distribution at Arecibo displayed in Figure 12, where it can be seen that meteors are detected
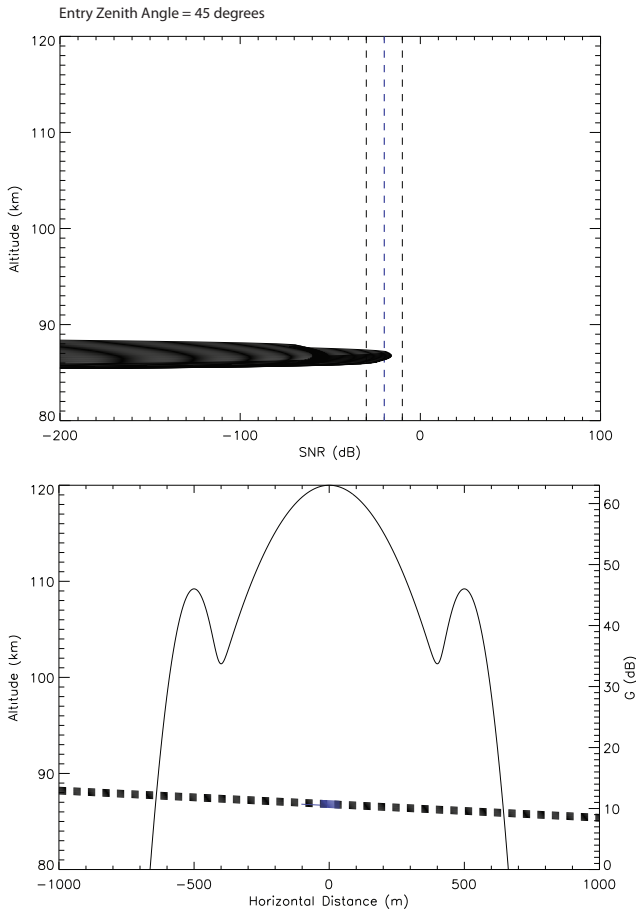
Figure 8. S/N and trajectory plots for a particle with mass equal to 5 μg, zenith entry angle equal to 45° and velocity equal to 11 km s^{-1} traveling through the center of the radar beam.

(A color version of this figure is available in the online journal.)

between 75 and almost 140 km of altitude (i.e., $H \sim 65$ km). However, the very high altitude meteors ($h > 130$ km) seem to be outliers suggesting to be rare events and thus we adopt a more conservative value of 55 km. Δx was defined in Section 2.3 as the horizontal distance from the center of the beam to the outer edge of the first side lobe (700 m).

Figure 13 shows $P(m, V, \alpha)$ as a function of meteor velocity for a particle mass equal to 10 μg and for four entry zenith angles. It is evident from this figure that for the particles traveling at zenith angles of 20°, 40°, and 60° the probability varies similarly while the meteoroid velocity is lower than 27 km s^{-1}. For instance, for these angles at $V = 11$ km s^{-1} the probability of detection is about 1%, rapidly increasing to 10% with only a $\sim$4 km s^{-1} increase in velocity, and reaching $\sim$25% for velocities equal to 27 km s^{-1}. For these angles, the highest probability is 80%. However, the steeper the entry angle is, the less velocity is needed to achieve the maximum value. For the case of particles with entry angle equal to 80°, the atmospheric filtering effect is evident, with particles having zero probability if their velocity is lower than 20 km s^{-1}. In fact this is true for entry angles equal or greater than 65°. At these large entry zenith angles, the particles are detected only when the velocities are high enough to ablate the main elements, at which point they have a high chance of detection ($\sim$70%). A more general view of these results is presented in Figure 14 where contour plots of the probability as a function of meteoroid mass and velocity are shown. Each of the panels represent a different entry

angle specified at the top of the panel. It can be seen from this figure that for a chosen Arecibo detection threshold of -20 dB, meteors will have 50% or higher probability of detection for masses greater than 10 μg and velocities greater than 25 km s^{-1} and for the case of large entry angles, particles will never be detected if their velocity is lower than 25 km s^{-1}.

The atmospheric filtering effect due to the meteor entry angle is clearly shown in Figure 15, where contour plots of the probability as a function of meteoroid mass and entry angle are displayed for six entry velocities. It can be first observed from the panels in this figure that for zenith angles greater than 80°, the probability is zero for almost all velocities except when the entry speed is very high, which extends the allowed entry angle up to 85°. At 11 km s^{-1}, particles are practically unobserved unless the masses are greater than 50 μg, in which case the probability is 10%–20% only when particles travel practically vertical with respect to the local zenith. Only when the velocity is greater than 14–15 km s^{-1} does the probability increase for larger entry angles, although it remains low in particular for those masses that represent the majority of ZoDy's predicted particle flux.

4. IMPLEMENTATION TO THE ZODIACAL DUST MODEL

As discussed earlier, the work presented here is motivated by the findings reported in Nesvorný et al. (2010), which predict that low-speed (11–20 km s^{-1}) particles with masses of the order of 1–10 μg represent 90% of the total meteoroid mass flux into the Earth's atmosphere and are largely undetected by meteor radars, in particular AMOR and CMOR (Nesvorný et al. 2011a). In this section we will use the results derived in Sections 2 and 3 to (1) determine if this flux can be detected by the much more sensitive Arecibo radar and its head echo observing technique; and (2) if that is the case, then to estimate what portion of the Arecibo meteor observations can be modeled with this flux in order to further quantitatively constrain ZoDy with ground-based observations.

To perform this validation we must first consider the fact that the Arecibo radar lacks interferometry capabilities, and thus the observations do not have information regarding direction. This implies that they only provide line-of-sight (vertical for the Arecibo case; Janches et al. 2003) velocity information (V_R in Figure 16). Furthermore, although we have reported mass information from these observations in the past (Janches et al. 2000b), those results are not optimal for the level of accuracy required in this work. This is due to the fact that the mass is calculated with the meteor momentum equation (Bronshten 1983) using the measured meteoroid deceleration. Because Arecibo does not have interferometric capabilities, it was assumed that the measured radial deceleration was the absolute deceleration, which can introduce large uncertainties. Also this "dynamical" mass determination technique can have up to an order of magnitude differences with those determined using more sophisticated methods (Close et al. 2005). Thus, instead of correcting the Arecibo observations with the detection bias resulting from the probability calculated in Section 3 and compare them with ZoDy's predictions, we do the reverse—we see what portion of the ZoDy particle flux should be detected by Arecibo and compare these predictions with the actual observations.

Currently ZoDy provides the total number of meteors that cross the Earth's cross section during the entire year as a function of particle mass, entry velocity, and radiant (in ecliptic
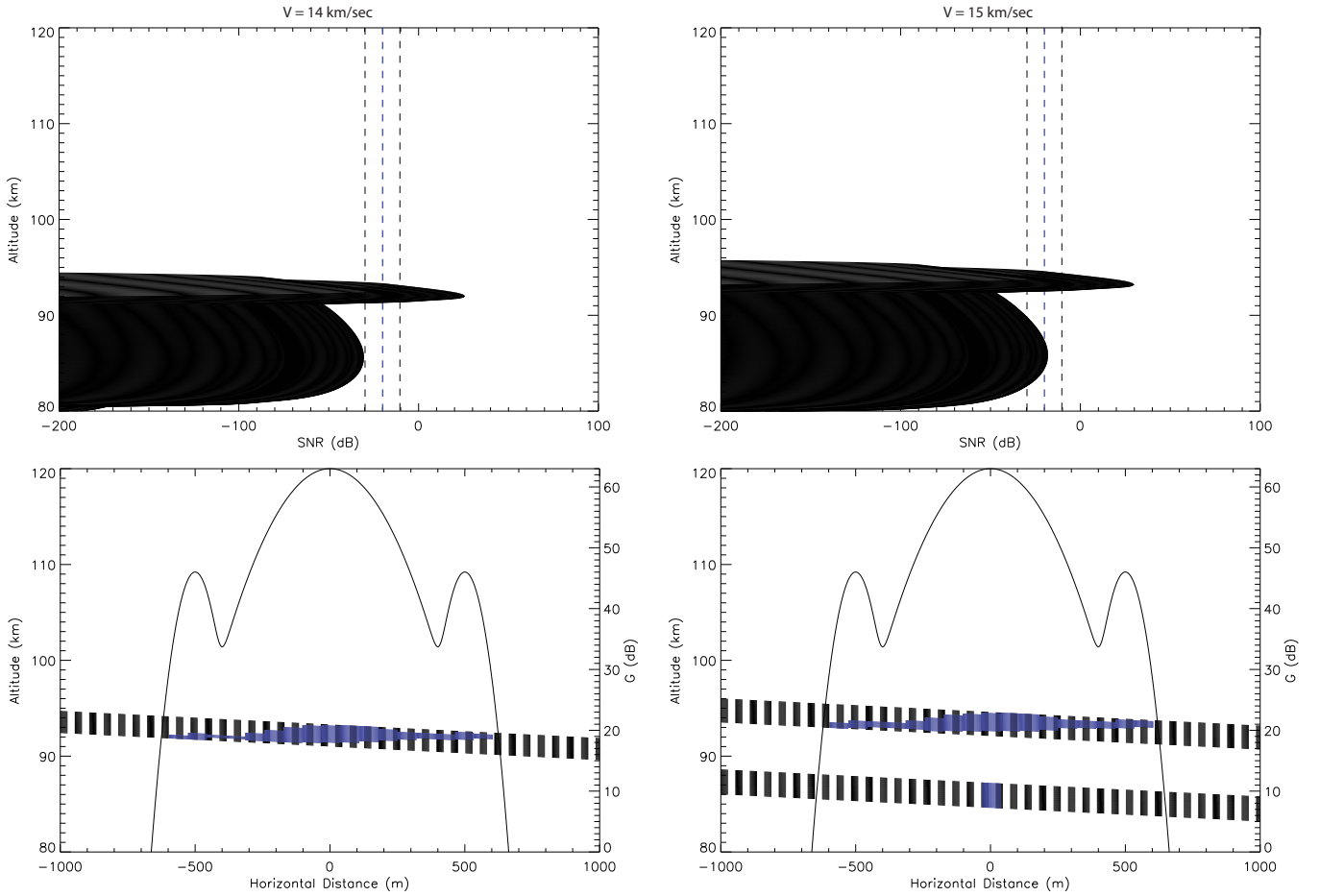
Figure 9. S/N and trajectory plots for $10\,\mu$g particles entering at $V = 14$ km s^{-1} (left panels) and 15 km s^{-1} (right panels) and an $\alpha = 45°$ traveling through the center of the radar beam.

(A color version of this figure is available in the online journal.)

coordinates). We will refer to this number as $N(m, V, \lambda, \beta)$ and thus ZoDy's flux (i.e., particles per unit area and per day) is given by

$$F(m, V, \lambda, \beta) = \frac{N(m, V, \lambda, \beta)}{365.25 \times \pi R_{\text{Earth}}^2}, \qquad (12)$$

where R_{Earth} is the Earth's radius, m is the particle mass provided in 28 bins ranging from 10^{-5} to 30 mg, V is the particle absolute geocentric velocity ranging from 11.5 to 71.5 km s^{-1} every 1 km s^{-1}, and λ and β are the ecliptic longitude and latitude, respectively, of the meteoroid's radiant provided every two degrees in both directions. Although the input velocity distribution includes the full spectrum of possible meteor speeds for particles with Sun-bound orbits, it is heavily weighted toward the slow speeds (Figure 1). For the purpose of this work, we will focus on comparing ZoDy's results with two quantities observed by Arecibo: the daily rates and the meteor line-of-sight velocity distributions. Both quantities are strongly dependent on the time of day and day of year (Janches et al. 2006; Fentzke & Janches 2008). To perform these tasks, we first calculate what portion of $F(m, V, \lambda, \beta)$ occurs over Arecibo during a relatively short- ($\Delta t \sim$ 1–5 minutes) period of time. In addition, we calculate the instantaneous local zenith angle of λ and β during this short period in order to estimate the meteoroid entry angle and thus obtain the radial velocity. Once these variables are calculated, they need to be "biased" by their probability-of-observation

using the methodology derived in the previous sections. For this, we assume that the portion of the incoming flux that will be detected is given by

$$n_p(m, V, \lambda, \beta, \alpha(t)) = F(m, V, \lambda, \beta) \times A_1(\alpha(t)) \\ \times P(V, \alpha, m) \times \Delta t. \qquad (13)$$

Replacing Equation (11) in Equation (13) results in

$$n_p(m, V, \lambda, \beta, \alpha(t)) = F(m, V, \lambda, \beta) \times A_2(m, V, \alpha(t)) \times \Delta t, \qquad (14)$$

becoming independent on assumptions regarding the beam size.

The comparison between Arecibo observations and ZoDy are shown in Figure 17. In the top panel of this figure, the detected meteor rates between approximately 6 pm on 2002 January 21, and 8 am local time of the next day are shown. This represents the diurnal behavior typically measured by HPLA radars, although seasonal differences are also present and their magnitudes strongly depend on geographical location (Janches et al. 2006; Fentzke et al. 2009; Sparks et al. 2009; Pifko et al. 2013). The predicted detected rates utilizing the methodology described in this paper are also presented in the same panel. To obtain these predictions, we utilize two different radar S/N thresholds (-10 and -20 dB) to estimate what portion of the flux provided by ZoDy will be detected by Arecibo. It can be seen from these panels that the predicted fluxes are much larger than those observed. The results show that at a
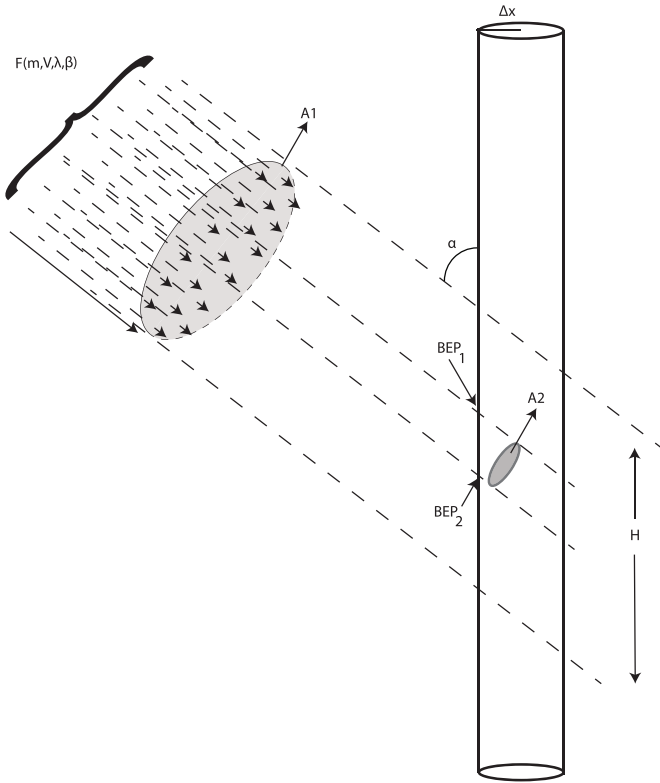
Figure 10. Schematic of our probabilistic approach.
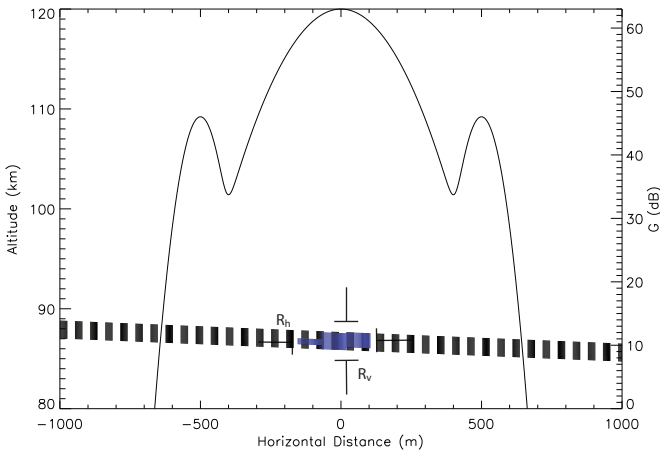

Figure 11. Definition of horizontal and vertical distances chose to calculate A2 displayed in Figure 10. This example corresponds to a particle with $m = 10\,\mu$g, $V = 11$ km s^{-1}, and $\alpha = 60°$.

(A color version of this figure is available in the online journal.)

Figure 12. Observed altitude distribution with the Arecibo radar during the 2002 observing campaign. Observations are clearly present in the 75–130 km altitude range, which results in $\Delta h = 55$ km.

Figure 13. Detection probability as a function of meteor velocity for a particle with $m = 10\,\mu$g for four different entry angles.

detection threshold of -20 dB, the detection rate should be 19 times larger than what Arecibo actually observes, while at a more conservative threshold of -10 dB it should be nine times larger than the observed rates. The bottom panel of Figure 17 shows a comparison between the predicted line-of-sight velocity distributions for the chosen detection thresholds and the actual Arecibo observations. That is, the predicted radial distribution includes only those meteors from ZoDy that are predicted to be detected by Arecibo and not all the meteors originating from ZoDy's flux. In this panel, the vertical axis is presented in logarithmic scale due to the large difference between prediction and observations. As can be seen in this panel, if the incoming flux is that described by ZoDy then the Arecibo observed distributions should be heavily dominated
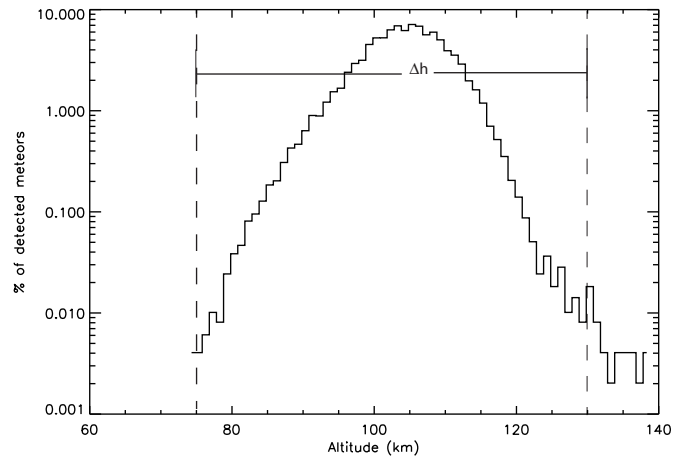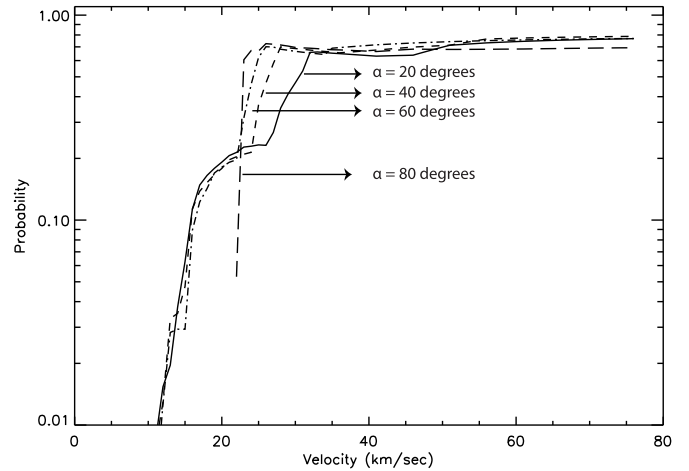
by low-velocity particles, with a clear peak between 11 and 15 km s^{-1}. At these velocities, ZoDy predicts 240 times more detections than what Arecibo observes at the lower detection threshold and 100 times more detections at -10 dB.

It is important to note that besides the lack of agreement at low velocities, the total lack of agreement in the high-velocity end of the distributions is due to the fact that currently ZoDy does not include most of the populations that provide the faster ($V > 30$ km s^{-1}) particles. JFC particles are what is currently included in the model because those provide a good fit to the zodiacal cloud thermal emission and helion/anti-helion meteors (Nesvorný et al. 2010, 2011a, 2011b). Future efforts will require the inclusion of particles from asteroid belt, Halley-type comets, and OCCs. The latter two sources will be the most relevant to the high-velocity portion of the radar observations. In particular, preliminary studies reported by Nesvorný et al. (2011b) explored small debris particles produced by OCC disruptions to determine whether the imprints of a hypothetical population of OCC meteoroids can be found in the existing meteor radar data. It was determined by those authors that about 1% of these particles orbitally evolve by Poynting–Robertson drag to reach orbits with a semimajor axis of 1 AU. This leads to a hypothesis regarding the long-standing problem in meteor science related to the relative strength of apex and H/AH sources: that the
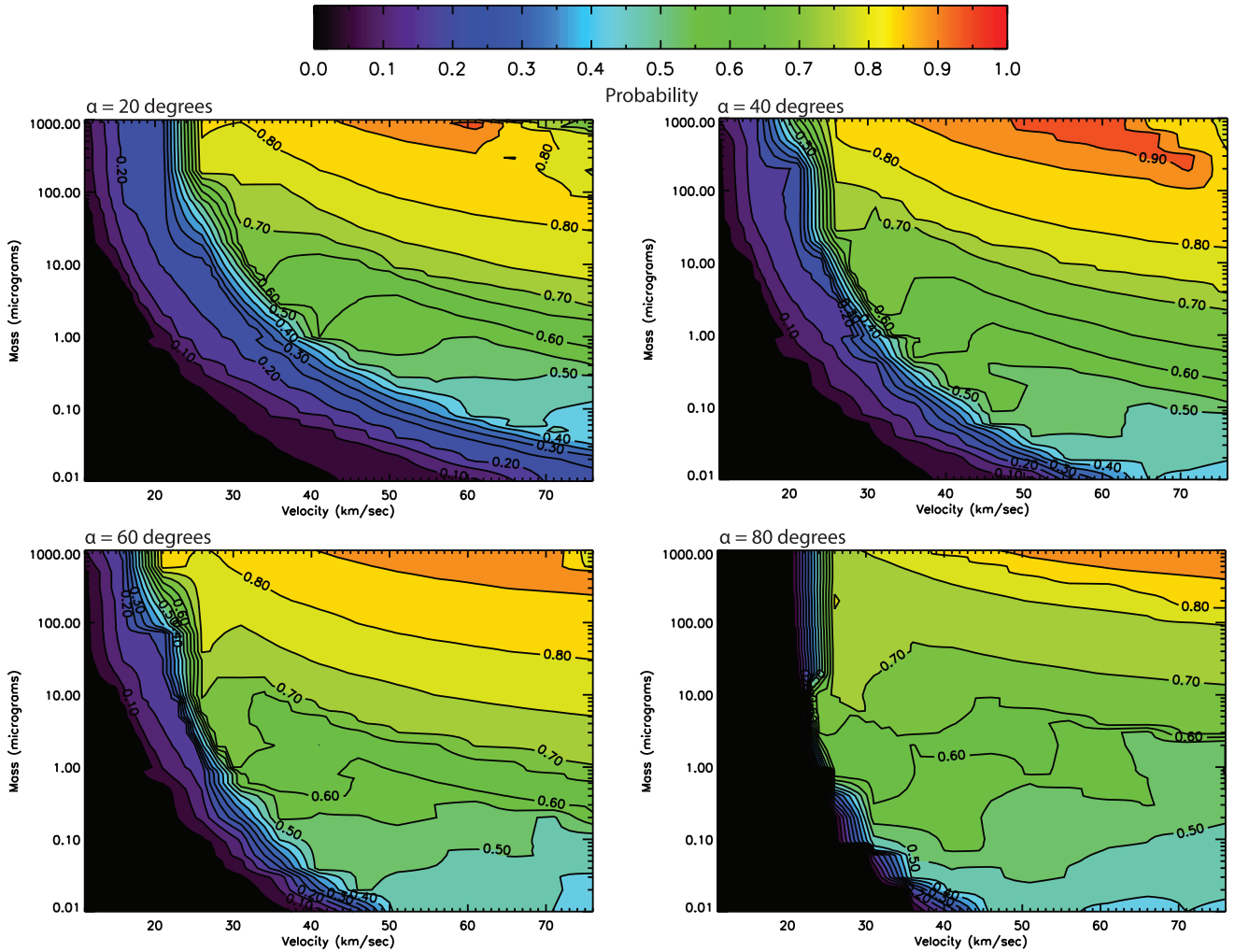
Figure 14. Contour plot of probability of detection for all masses and velocities considered in this work for a S/N threshold of -20 dB and four different entry angles. The atmospheric filtering effect is evident at $\alpha = 80°$.

(A color version of this figure is available in the online journal.)

reason why apex meteors are more prominent in observations of highly sensitive radars can be related to orbital dynamics of particles released on the long-period orbits. However, even when these sources are included, the lower velocities should still be dominant according to Nesvorný et al. (2010), and the disagreement between ZoDy and the Arecibo observations will remain.

5. DISCUSSION

5.1. Potential Sources for Disagreements: The Need for a Revised β_{ip}

In the previous sections we described a new method for estimating the sensitivity of the 430 MHz radar to detect meteor head echoes produced by small and slow extraterrestrial particles and used those results to assess the probability of detection as a function of particle mass, velocity, and entry angle. We then weighted the meteor flux predicted by ZoDy in order to examine what portion of the Arecibo observed distribution should be attributed to the ZoDy flux. With our current knowledge of meteor ablation and ionization, we have estimated that the Arecibo detections should be heavily dominated by the ZoDy flux, at least an order of magnitude higher than the

actual observations. In principle, one could argue that such results suggest that ZoDy's description of the ZDC needs revision. However, besides the strong constraint by *IRAS* observations reported by Nesvorný et al. (2010), the meteoric mass input rate of 30–40 t d^{-1} of slow particles predicted by ZoDy is able to explain several atmospheric phenomena related to the meteoric flux. For example, Marsh et al. (2013); Feng et al. (2013), and Langowski et al. (2014) recently described global modeling of the mesospheric Na, Fe, and Mg/Mg$^+$ layers, respectively, using the meteor input function (MIF) developed by Fentzke & Janches (2008). The authors showed that in order to find agreement between the model and observations for these three metals, the MIF had to be artificially scaled because the larger average speed predicted by the MIF ($\sim$25–30 km s^{-1}) does not produce the degree of differential ablation observed in these layers (Plane 2003). A larger and slower MIF, as predicted by ZoDy, would, in principle, produce the degree of differential ablation required to model the Fe, Mg, and Ca mesospheric layers at the same time as the Na layer, without artificially reducing their injection rates. In addition, the ZoDy flux produces a sensible input rate of cosmic spherules and the correct optical extinction of meteoric smoke in the mesosphere (these topics will be treated in a forthcoming publication). Thus, these
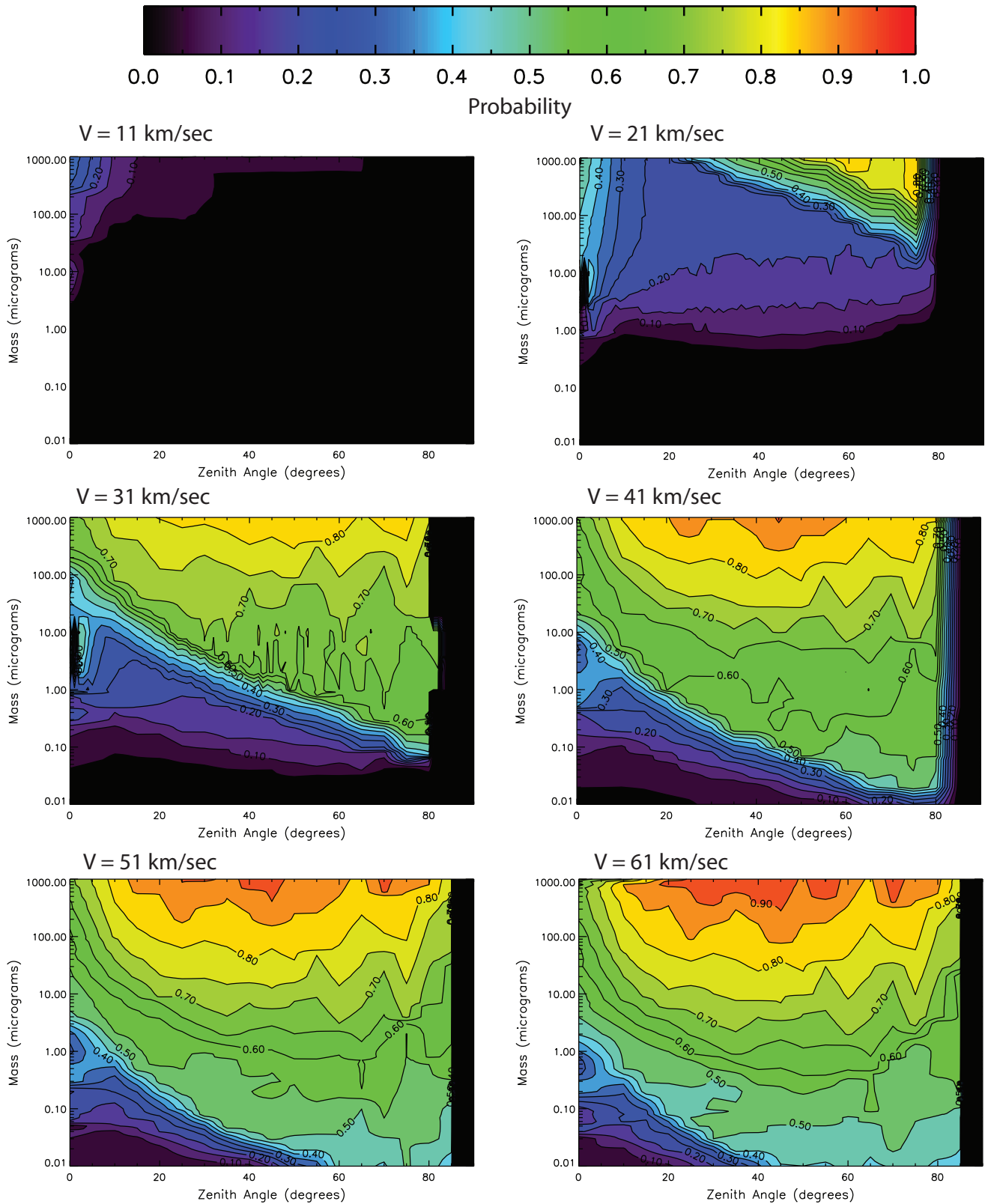
13

Figure 15. Contour plot of the probability of detection for all masses and angles considered in this work for an S/N threshold of −20 dB and six different entry velocities.

(A color version of this figure is available in the online journal.)

arguments, together with the strong agreement found with *IRAS* spectral measurements, motivate a deeper exploration of possible reasons for the disagreement between ZoDy and Arecibo's observations.

In order to first understand these results, we show in Figure 18 a comparison between the characteristics of the ZoDy flux that travels through the Arecibo beam, which we refer here as the input distributions, and the portion that is predicted to be
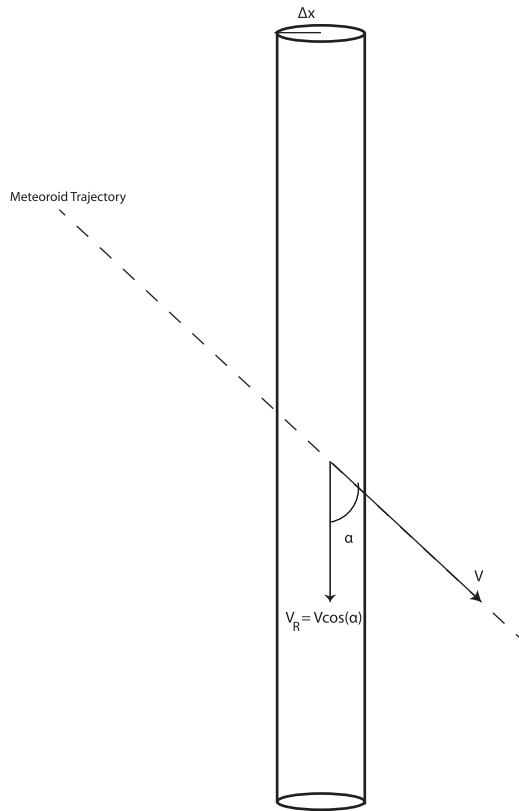
Figure 16. Definition line of sight (i.e., radial) and absolute meteor velocity.
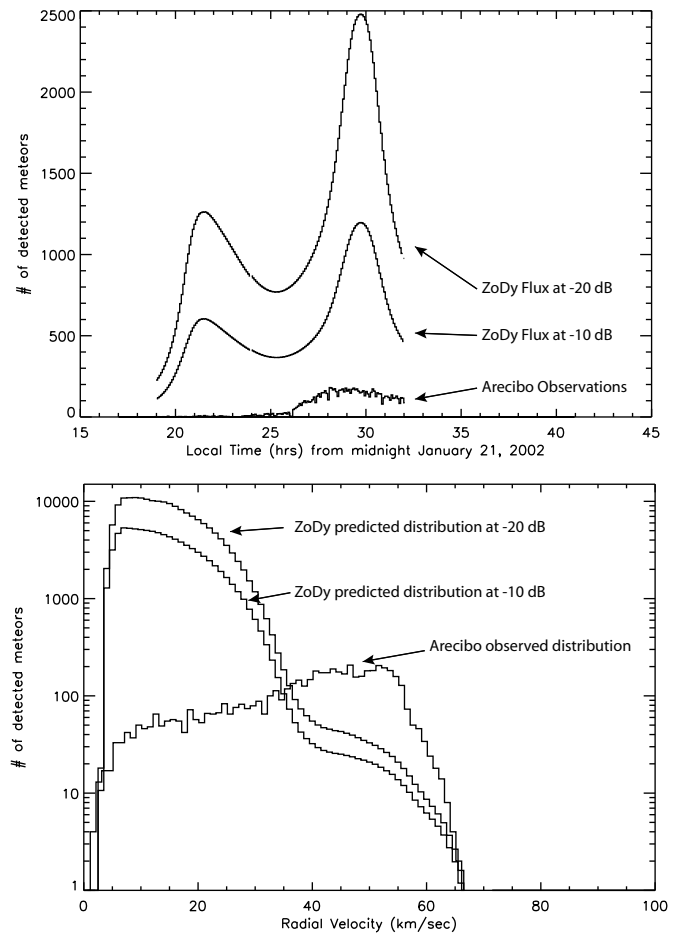

Figure 17. Top: comparison between predicted detected meteor rates assuming ZoDy to be the incoming flux and those observed by Arecibo. Bottom: comparison between predicted radial velocities of detected meteors assuming ZoDy to be the incoming flux and those observed by Arecibo.

Table 1
Percentage of Number and Mass Input Contributed by Particles
with Masses Smaller than $1\,\mu$g

β_{ip}	Threshold (dB)	Number ($m < 1\,\mu$g) / Total	Mass ($m < 1\,\mu$g) / Total
Jones (1997)	-10	0.54	0.04
	-20	0.67	0.07
Revision 1	-10	0.27	0.01
	-20	0.38	0.02
Revision 1	-10	0.3	0.02
	-20	0.67	0.07

detected by Arecibo. The top panel shows the absolute velocity distributions while the bottom panel shows the mass distribution. As expected, the input distributions reflect ZoDy's main characteristics with a velocity distribution heavily weighted toward meteors with absolute speeds of 12–14 km s^{-1}. As can be seen in the top panel, less than 1 in 10^5 of these particles are detected by Arecibo. In fact, the slow line-of-sight velocity distribution predicted to be detected by Arecibo (Figure 17, bottom) is comprised of particles with an absolute velocity distribution peak of $\sim$30 km s^{-1}, even though particles are detected with velocities as low as 11 km s^{-1}, which are the typical radar-detected velocities of meteors originating from the helion and anti-helion Sporadic Sources (Fentzke & Janches 2008). Furthermore, although ZoDy's input includes masses as low as $10^{-3}\,\mu$g, the *IRAS* measurements are effectively constrained by particles with masses between 1 and $10\,\mu$g. Thus the distribution below about $1\,\mu$g is essentially unconstrained, except that it is known that small particles do not contribute to the ZDC IR emission due to the featureless nature of its spectrum. The manner in which ZoDy mimics the continuous distribution of particles as a function of size, $N(D)$, is by parameterizing this quantity as a power law given by

$$dN(D) = N_0 \times D^{-a} dD, \qquad (15)$$

where N_0 is a normalization constant and a is the mass index of the distribution. ZoDy assumes $a = 2.9$. Because of Arecibo's sensitivity, it could be argued that the excess in predicted detections is at least in part due to the large amount of small unconstrained particles in the model. This is explored in the bottom panel of Figure 18, where the number of meteors as a function of their mass is displayed for the input and detected distributions. While particles greater than $1\,\mu$g suffer a decrease

of about an order of magnitude between input and detection, the difference increases significantly for lower masses. In fact, while the number of particles with masses lower than $1\,\mu$g represent 99% of the input distribution, their contribution is reduced to 67% and 54% in the detected distributions for the -20 and -10 dB thresholds. In terms of the mass input, these numerous particles provide 50% of the input and only 4% and 7% of the detected mass for both thresholds (Table 1). Thus, a potential solution to reach better agreement would involve reducing the exponential in the size distributions of small particles. Although not shown here, we have performed this sensitivity study introducing a shallower distribution ($a = 2$) for particles with diameter lower than $100\,\mu$m. Because the whole population had to be re-calibrated to match *IRAS* fluxes, this change results in an accretion rate slightly larger than in
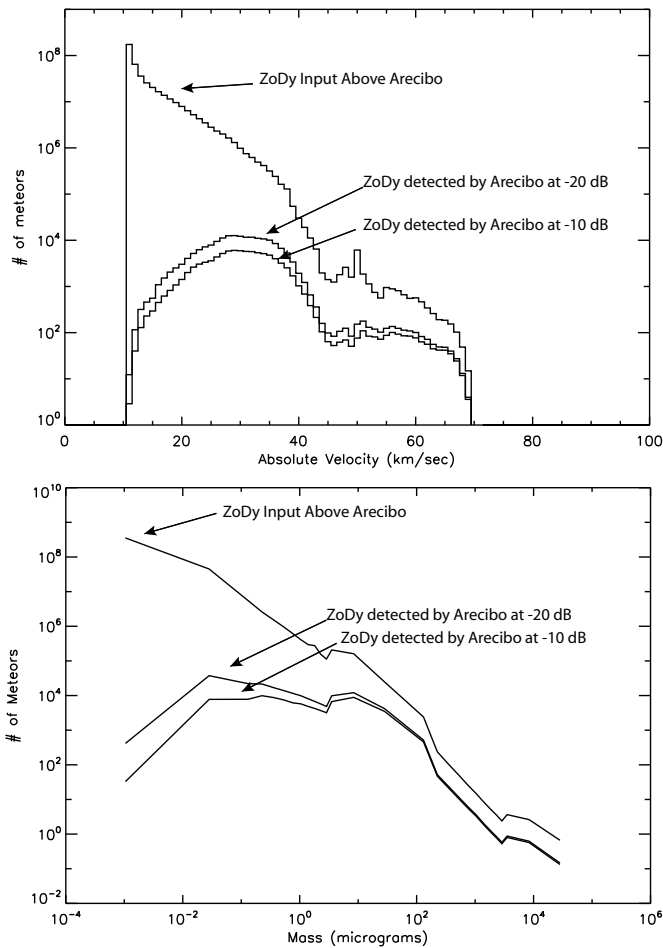
Figure 18. Top: comparison between the distribution of absolute velocities of meteors traveling through the radar beam predicted by ZoDy and those predicted to be detected by the radar using our approach. Bottom: comparison between the distribution of meteors masses input by ZoDy and those predicted to be detected by the radar using our approach.

the original distribution and the overall result is an increase in the discrepancy between Arecibo observations and ZoDy. A simpler approach is to invoke the stated 50% uncertainty on ZoDy's prediction (Nesvorný et al. 2010, 2011a). However, it is evident from the results presented in Section 4 that reducing the influx by a factor of two would not suffice to obtain agreement and most likely the solution must be found in our treatment of the detectability.

5.2. Revision of β_{ip}

In this section, we will explore the origins of the extensively used β_{ip} value derived by Jones (1997),[8] which is based on experiments involving the firing of high-velocity Fe particles into a chamber of air at low pressure and measuring electron production along the particle track. These experiments reported in Friichtenicht & Becker (1973) are a rather indirect way of measuring ionization efficiency because the rate of ablation of Fe from the particles has to be inferred from the deceleration of the particles. Nevertheless, Jones (1997) used these experiments combined with data on meteor luminosity and radar scattering to derive expressions for the ionization efficiency of the major

elements. As stated by the author, however, the expressions reported in that work overpredicted the ionization efficiency by an order of magnitude[9] (Jones 1997).

In this work, we re-estimate β_{ip} as a function of collision energy by utilizing measurements of the ionization cross section of K atoms in collision with O_2 and N_2 over the full range of collision energies reported by Cuderman (1972). This is the only metal atom for which there is experimental data with both collision partners over a wide collision energy and a detailed description of how the absolute cross sections were measured. The results show that charge transfer with O_2 is much more important than with N_2: the K + N_2 cross section is at least one order of magnitude less than that for O_2, so in-air N_2 collisions cause a 5% contribution to the total ionization at a collision velocity of 11 $km\,s^{-1}$, increasing to a 16% contribution at 72 $km\,s^{-1}$. Although about 70% of the product is O_2^- rather than free electrons at the relatively low maximum impact velocities employed in a study by Moutinho et al. (1971), the O_2^- will be produced with sufficient translational speed (and internal vibrational excitation) to auto-detach the electron since the electron affinity of O_2 is only 0.45 eV. Thus we assume that the final products of these collisions are K^+ and e^-.

In order to compute β_{ip}, the ionization cross section is first divided by the cross section for momentum-changing collisions to produce a single collision ionization probability β_0; β_0 is then increased to allow for ionization through subsequent collisions of the metal atom as it loses momentum (Jones 1997). In order to estimate the momentum-changing collision cross section, we employed quantum chemistry trajectory calculations. The hybrid density functional/Hartree–Fock B3LYP method was employed from within the Gaussian 09 suite of programs (Frisch et al. 2009), combined with the 6-311+G(2d) triple zeta basis set. This is a large, flexible basis set that has both polarization and diffuse functions added to the atoms. Classical trajectories were performed using the atom centered density matrix propagation molecular dynamics model (Schlegel et al. 2002). Trajectories were initiated at relative velocities of 11–72 $km\,s^{-1}$. One definition of a momentum-changing collision is that it is inelastic, i.e., there is a transfer of collisional kinetic energy into internal vibrational energy of the O_2. The maximum impact parameter b_{max} was then determined for collisions in which the O_2 after the collision possessed just one vibrational quantum. On the doublet surface for K + O_2, the average over the range of collision velocities is $b_{max} = 2.9\,\text{Å}$ (b_{max} increases by only 20% when V increases from 11 to 72 $km\,s^{-1}$). For the less reactive quartet surface, $b_{max} = 2.0\,\text{Å}$. Statistically, reaction on the quartet surface is twice as likely as on the doublet surface, so overall for K + O_2, $b_{max} = 1/3 \times 2.9 + 2/3 \times 2.0 = 2.3\,\text{Å}$. For K + N_2, $b_{max} = 1.8\,\text{Å}$. These impact parameters are treated as independent of collision velocity. The momentum-changing cross section is then given by πb_{max}^2. Figure 19 (top panel) illustrates β_0 for O_2 and N_2 as a function of collision velocity, calculated from the ionization cross sections of Cuderman (1972). Also shown in this figure are fits to the experimental data points using the analytic expression of Jones (1997):

$$\beta_0(V) = \frac{c(V - V_0)^2 V^{0.8}}{1 + c(V - V_0)^2 V^{0.8}}, \qquad (16)$$

---

[8] For the case of CABMOD, Vondrak et al. (2008) used the analytic expression for how this parameter varies with collision energy, but determined it for individual elements.

[9] (Jones 1997) abstract concludes "The observational ionization coefficients are much lower than predicted by the present theory and we provisionally explain this as a consequence of transfer of charge from the meteoric ion to a molecule of the air."
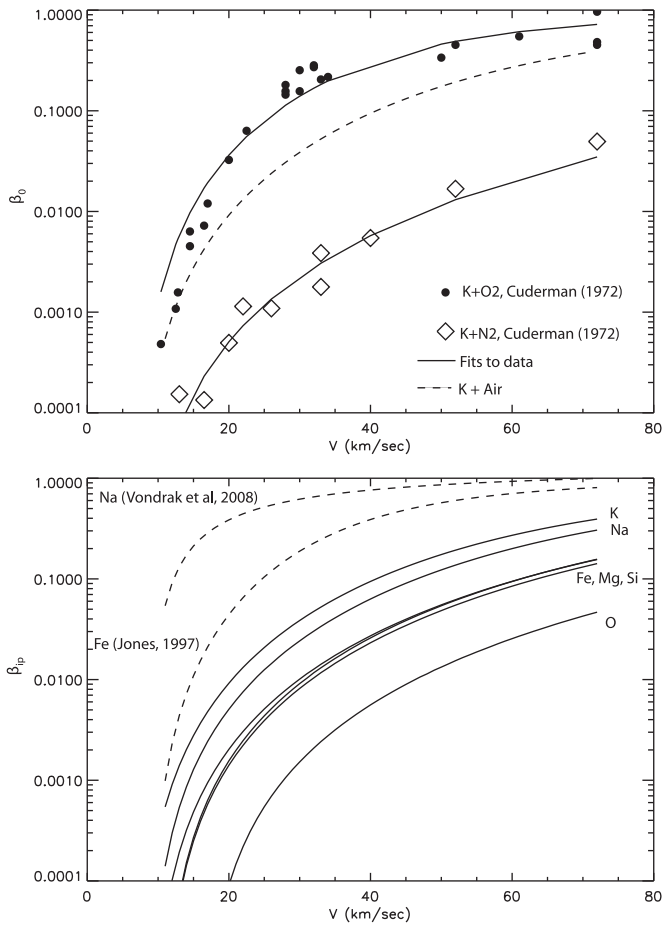
Figure 19. Top: β measured by Cuderman (1972) for K + O$_2$ and K + N$_2$. The solid lines through the experimental points are fits of the expression from Jones (1997). The dash line is the estimated β_0 for K + air collisions, which includes the correction for multiple high energy collisions. Bottom: variation of β_{ip} for all the meteoric atoms colliding with air, as a function of particle velocity.

Table 2
Fitted Parameters for Calculating β_{ip} as a Function of V

Atom	$c/(\text{km s}^{-1})^{-2.8}$	$V_0/(\text{km s}^{-1})$
K	5×10^{-6}	7.0
Na	3.6×10^{-6}	8.6
Mg	1.6×10^{-6}	10.6
Fe	1.5×10^{-6}	9.0
Si	1.4×10^{-6}	10.5
O	5.1×10^{-7}	16.0

where V_0 is the threshold velocity given by

$$V_0 = \sqrt{\frac{2(M_e + M_a)e\psi}{M_e M_a}}, \qquad (17)$$

where M_e and ψ are the mass and ionization potential of the atom (K, in this case), respectively, e is the electronic charge, and M_a is the molecular mass of O$_2$ or N$_2$. c is a fitted parameter.

In the atmosphere, K has a 20% chance of collision with an O$_2$. β_0 for air is then obtained as $0.2\beta_0$ (O$_2$) + $0.8\beta_0$ (N$_2$). The composite fit of Equation (16) for K in air is then achieved with $c = 5 \times 10^6$ (km s^{-1})$^{-2.8}$, $V_0 = 7$ km s^{-1} (an average between 6.9 km s^{-1} for K + O$_2$ and 7.1 km s^{-1} for K + N$_2$). β_{ip} is then given by Jones (1997):

$$\beta_{ip}(V) = \beta_0(V) + 2 \int_{V_0}^{V} \frac{\beta_0(V')}{V'} dV'. \qquad (18)$$

The resulting curve of β_{ip} versus V_0 for K + air collisions is also shown in Figure 19.

There is some experimental data available for Na + O$_2$ and N$_2$ collisions (Bydin & Bukteev 1960; Moutinho et al. 1971; Kleyn et al. 1978), but the absolute cross sections are not consistent, although the Na ionization cross sections are clearly smaller than the corresponding K cross sections. Therefore, in order to

determine β_{ip} for Na and other meteoric metals, we adopt the following approach. The maximum interaction distance between a metal atom and a collision partner is given by the curve-crossing (or harpoon) distance (Smith 1980),

$$R_c = \frac{e(\psi - \gamma)}{4\pi \epsilon_0}, \qquad (19)$$

where γ, the vertical electron affinity of O$_2$ and N$_2$, is close to zero. The ionization cross section is likely to scale as R_c^2, particularly at high V where threshold effects are small. We therefore estimate c for Na, Mg, Fe, Si, and O by dividing $c = 5 \times 10^{-6}$ (km s^{-1})$^{-2.8}$ for K by factors of 1.4, 3.1, 3.3, 3.5, 9.8, respectively. V_0 for each element from its respective ψ (Equation (17)). The values of c and V_0 for calculating $\beta_{ip}(V)$ using Equations (16) and (17) are listed in Table 2.

The resulting β_{ip} for the six elements are plotted against V in Figure 19 (bottom panel). This shows that, compared to previous estimates (Jones 1997; Vondrak et al. 2008), the ionization efficiencies are about two orders of magnitude lower for Na and K at speeds below 20 km s^{-1}, and slightly less than one order of magnitude lower for the main elements (Fe, Mg, Si, and O) at higher speeds.

5.3. Modeled Results Utilizing the Revised β_{ip}

Figure 20 shows the same results as Figure 17 but utilizing the revised values of β_{ip} shown in the bottom panel of Figure 19 which we refer to as Revision 1 in Table 1. As can be seen in these figures, although improvement is achieved, ZoDy still predicts a flux that should dominate the Arecibo meteor rate and velocity distributions. In particular, at a detection threshold of -20 dB, ZoDy predicts that Arecibo should detect three times more particles that is actually observed, while at -10 dB they would represent 1.3 times the detected rates. Once again we emphasize that the final disagreement will be even greater because ZoDy does not include the populations that would produce most of the detected particles by Arecibo (high-speed). In terms of the radial velocity distributions, the ZoDy flux should provide a peak at $\sim$7 km s^{-1} that is 10–80 times larger than those currently detected.

As discussed above, β_{ip} is calculated by dividing the ionization cross section by the cross section for momentum-changing collisions between the metal atom and the air molecule (O$_2$ or N$_2$). The requirement that a momentum-changing collision has to be inelastic (i.e., arising from translational–vibrational energy transfer) may be too restrictive, since elastic collisions at large impact parameters will makes small changes to the momentum of the metal atom. The upper limit to the cross section for interaction between a metal atom and O$_2$ or N$_2$ molecules is given by πR_c^2 (see Equation (19) for the definition of R_c). For K + O$_2$/N$_2$, R_c is about 48% larger than the distance required

Figure 20. Same as Figure 17 using the β_{ip} estimates resulting from Revision 1.
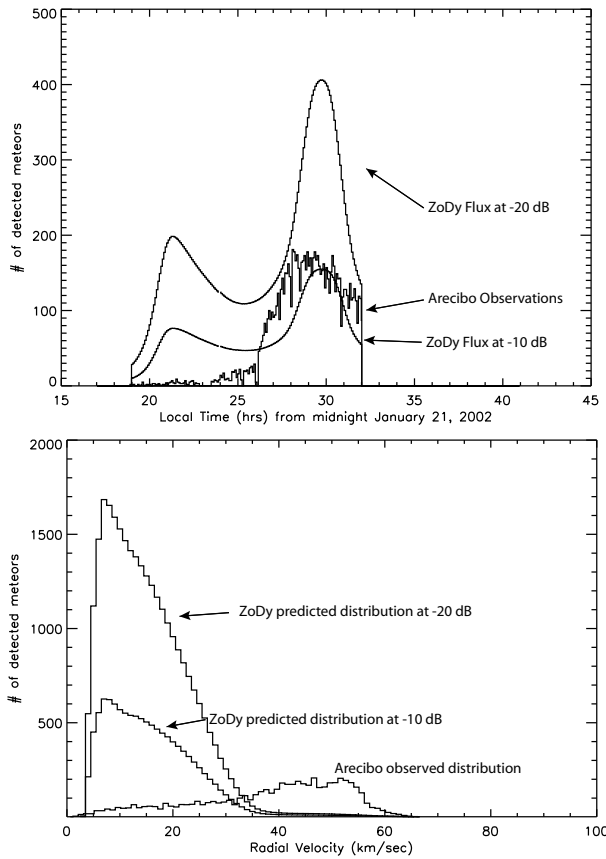

Figure 21. Same as Figure 17 using the β_{ip} estimates resulting from Revision 2.

to impart vibrational excitation (b_{max}), which would correspond to a decrease of β_{ip} by a factor of $1.48^2 \sim 2.2$ for K (and the other metal atoms, which are scaled to it). We refer to this lower limit of β_{ip} as Revision 2 in Table 1. The comparison between ZoDy predictions and Arecibo observations utilizing this second revision are displayed in Figure 21, where it can be seen that a much better agreement is found, particularly for a detected threshold of -10 dB. According to these results, if ZoDy provides most of the incoming flux, it would represent about 60% of the actual detected rates at the lower higher threshold. However, if we invoke the higher sensitivity (i.e., detection threshold of -20 dB), ZoDy should provide 1.6 times more meteors than are actually detected. Note that even at the -10 dB results, ZoDy predicts a rate of particles in the evening before midnight that is significantly larger (a factor of four) than those detected by the radar. If we take the lower limit to the ZoDy flux (50% uncertainty), then a reasonable agreement is obtained between model prediction and observations, in particular for the -10 dB detection threshold where they would represent about 30% of the observed rates and agree well with the diurnal distributions. Interestingly, ZoDy's particles originating from JFCs will have radiants mostly concentrated around the helion and anti-helion sporadic meteor sources (Nesvorný et al. 2010) and thus the 30% rate in the detections of particles coming from these sources is in good agreement with predictions of our earlier MIF model reported by Fentzke & Janches (2008). In terms of the radial velocity distribution, however, the disagreement is still significant.

To explore potential sources of improvement, we display in Figure 22 a comparison between the input and detected distributions predicted by ZoDy, similar to Figure 18, but for
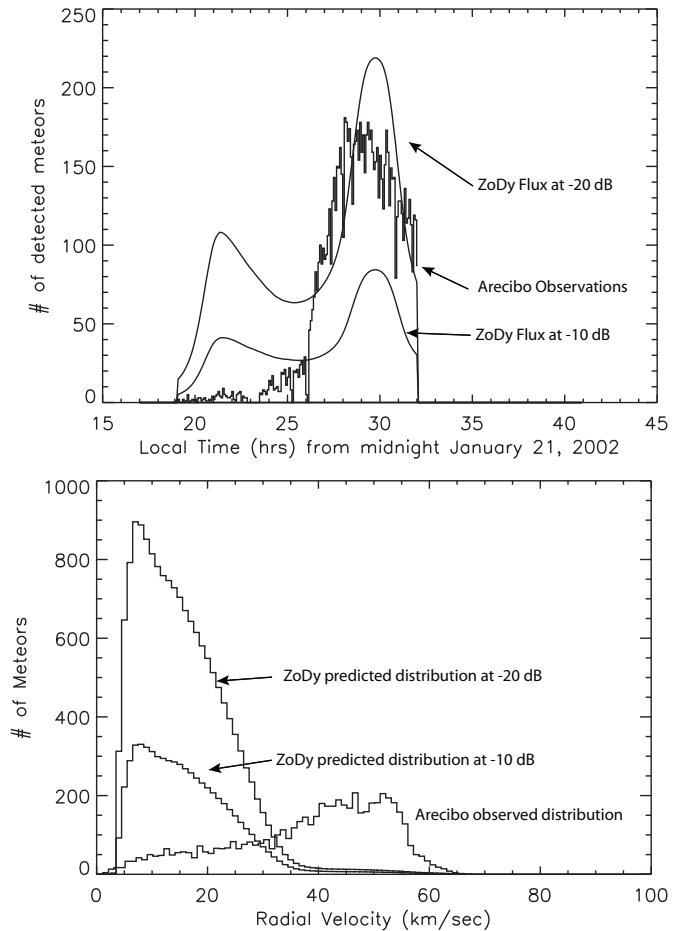
both revised estimates of β_{ip}. The solid lines in Figure 22 represent the results derived with Revision 1, while the dashed lines represent Revision 2. These panels show, as expected, that the revised estimates of β_{ip} contribute even more to filter out particles with masses lower than $\sim 1 \mu g$. However, for higher masses, the reduction of detected particles is not significant when compared to the results utilizing the original values of β_{ip}. Looking at the top panel of Figure 22, particles with velocities lower than 15 km s^{-1} were completely removed from the detected distributions. As discussed in Section 2.3, once the "larger" particles have speeds higher than 15 km s^{-1}, the S/N is much higher than the detection threshold, so that even if the ionization efficiency is close to its lower limit, these particles will be detected. So while these results do support ZoDy's main hypothesis that most of the 12–14 km s^{-1} particles with mass equal to 1–$10 \mu g$ could remain undetected, even by the most sensitive radar utilized for meteor observations, the number of particles with higher velocities entering the beam at larger zenith angles is too high and thus continues to dominate the predicted distributions. One potential solution is perhaps to explore the possibility to revised ZoDy such that the *IRAS* constraint is still met, but with a reduced contribution from particles with velocities larger than 15 km s^{-1}.

6. CONCLUSIONS

In this manuscript, we presented a new approach that aims at addressing the meteoric mass flux into planetary atmospheres in a comprehensive manner by combining models of dust release
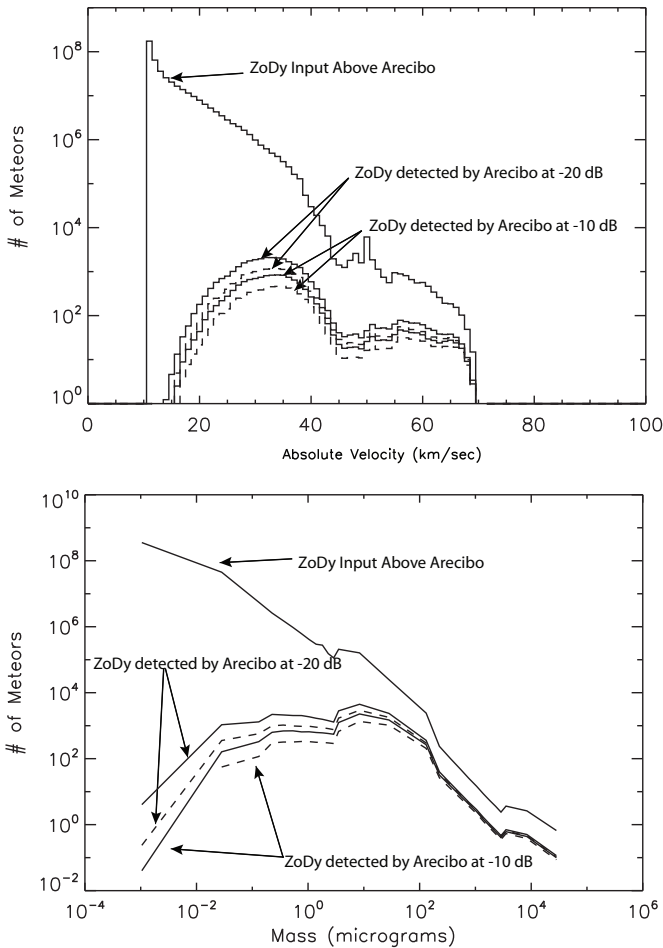
Figure 22. Same as Figure 18 using the β_{ip} estimates resulting from Revision 1 and 2.

from celestial bodies, orbital evolution, ablation, and ionization processes when dust particles encounter planetary atmospheres and ultimately by constraining these models simultaneously by all available observing techniques. We started with a recently developed physical model of the ZDC reported by Nesvorný et al. (2010) constrained with spectral observations of the ZDC provided by *IRAS* in order to predict the daily rates and radial velocity distributions that should be detected by a ground-based radar. In particular, we have compared these model results with head echo meteor observations obtained with the most sensitive radar in the world utilized to date for meteor studies—the Arecibo Observatory 430 MHz Radar located in Puerto Rico (Janches et al. 2008, 2014). We have also combined ZoDy with a new approach based on the CABMOD developed by Vondrak et al. (2008) to determine (1) the sensitivity of the radar to detect meteors produced by particles with a certain mass, velocity, and entry angle; and (2) the probability of detection based on the traveling conditions through the radar beam that such particles are required to have in order to be detected. We have found that using the meteor ionization probability, β_{ip}, derived by Jones (1997), which is universally utilized in radar meteor research (Close et al. 2002; Vondrak et al. 2008; Janches et al. 2009; Nesvorný et al. 2011a; Weryk & Brown 2013, among some assorted type of investigations), ZoDy overpredicts the Arecibo observed rates by 10–20 times and the peak of the slow portion of the line-of-sight velocity distribution by two to three orders of magnitude. This strong disagreement, however,

is due at least in part to the accuracy of the determination of β_{ip}, which, as argued by Jones (1997), is likely overpredicted by at least an order of magnitude. Further exploration on this issue leads to a re-estimation of β_{ip} as a function of collision energy, utilizing earlier measurements of the ionization cross section of K atoms over the full range of collision energies reported by Cuderman (1972) and demonstrating that, most likely, β_{ip} is about two orders of magnitude lower than the values reproduced by Jones (1997) for the case of Na and K at speeds below 20 km s^{-1} and slightly less than one order of magnitude lower for the main elements (Fe, Mg, Si, and O) at higher speeds. This revision leads to finding better agreement between ZoDy predictions and Arecibo observations. In particular, at a chosen S/N detection threshold of −10 dB and invoking the lower value of ZoDy's flux estimate (16 t d^{-1}), particles originating from JFCs, with radiants mostly concentrated around the helion and anti-helion sporadic meteor sources, would represent about 30% of the observed rates and agree well with the diurnal distributions. This percentage in the detections is in good agreement with predictions of our earlier MIF model reported by Fentzke & Janches (2008). One must be cautious with this agreement though, since an S/N threshold of −10 dB may be too conservative as Arecibo can detect meteors with up to 20 dB (two orders of magnitude) lower signal strength. However, even at this lower limit of the flux ZoDy overpredicts the slow portion of the Arecibo radial velocity distributions by a factor of three. A detailed investigation of the results by our new approach shows that particles with velocities lower than 15 km s^{-1} for most of the particle masses considered are mostly undetected as hypothesized by Nesvorný et al. (2010). The decrease in β_{ip}, however, does not produce significant differences for particles with masses greater than 1 μg and larger velocities. This produces a detected absolute velocity distribution with a peak at ∼30 km s^{-1} in agreement with those measured by radars from particles originating from the helion and anti-helion sources (Jones & Brown 1993; Galligan & Baggaley 2004; Fentzke & Janches 2008). However, the combination of the high number of these particles predicted by ZoDy together with the fact that they will mostly enter the Arecibo beam at some angle greater than zero produces a peak at slow radial velocities that is at best greater by a factor of three with respect to the observations. This implies that ZoDy requires some revision. In order to maintain the flux, a potential solution is a scenario with a steeper distribution where the number of particles with speeds lower than 15 km s^{-1} is increased while those with higher velocities are decreased.

In a second paper, we will apply our new approach to observations performed during other seasons, geographical locations, and additional HPLA radars with less sensitivity than Arecibo; explore how the current ZoDy predicts the observed seasonal and geographical distributions (Fentzke et al. 2009; Pifko et al. 2013); and compare what portion of the predicted flux contributes to the detections of the various systems utilized (Janches et al. 2008, 2014).

REFERENCES

Baggaley, W. 2002, in Meteors in the Earth's Atmosphere, ed. E. Murad & I. Williams (Cambridge: Cambridge Univ. Press), 123
Baggaley, W., Bennett, R., Steel, D., & Taylor, A. 1994, QJRAS, 105, 10353
Breakall, J. K., & Mathews, J. D. 1982, JATP, 44, 449
Bronshten, V. 1983, Physics of Meteoric Phenomena (Dordrecht: Reidel)
Brown, P., Weryk, R. J., Wong, D. K., & Jones, J. 2008, EM&P, 102, 209
Bydin, J. F., & Bukteev, A. M. 1960, SPTP, 5, 512
Campbell-Brown, M., & Wiegert, P. 2009, M&PS, 44, 1837
Chau, J. L., & Woodman, R. 2004, ACP, 3, 6063
Close, S., Brown, P., Campbell-Brown, M., Oppenheim, M., & Colestock, P. 2007, Icar, 186, 547
Close, S., Oppenheim, M., Durand, D., & Dyrud, L. 2005, JGRA, 110, 9308
Close, S., Oppenheim, M., Hunt, S., & Coster, A. 2004, Icar, 168, 43
Close, S., Oppenheim, M., Hunt, S., & Dyrud, L. 2002, JGR, 107, 1295
Cremonese, G., Borin, P., Lucchetti, A., Marzari, F., & Bruno, M. 2013, A&A, 551, A27
Cuderman, J. F. 1972, PhRvA, 5, 1687
Dyrud, L. P., & Janches, D. 2008, JASTP, 70, 1621
Feng, W., Marsh, D. R., Chipperfield, M. P., et al. 2013, JGRD, 118, 9456
Fentzke, J. T., & Janches, D. 2008, JGRA, 113, A03304
Fentzke, J. T., Janches, D., & Sparks, J. J. 2009, JASTP, 71, 653
Friichtenicht, J. F., & Becker, D. G. 1973, NASASP, 319, 53
Frisch, M. J., Trucks, G. W., Schlegel, H. B., et al. 2009, Gaussian–09 Revision D.01 (Wallingford, CT: Gaussian Inc.)
Galligan, D. P., & Baggaley, W. J. 2004, MNRAS, 353, 422
Galligan, D. P., & Baggaley, W. J. 2005, MNRAS, 359, 551
Hawkins, G. S. 1956, AJ, 61, 386
Hughes, D. W. 1978, in Cosmic Dust, ed. J. A. M. McDonnell (Chichester: Willey), 123
Hunt, S., Oppenheim, M., Close, S., et al. 2004, Icar, 168, 34
Janches, D., & Chau, J. 2005, JASTP, 67, 1196
Janches, D., Close, S., & Fentzke, J. T. 2008, Icar, 193, 105
Janches, D., Dyrud, L. P., Broadley, S. L., & Plane, J. M. C. 2009, GeoRL, 36, 6101
Janches, D., Heinselman, C., Chau, J., Chandran, A., & Woodman, R. 2006, JGR, 111, A07317
Janches, D., Hocking, W., Pifko, S., et al. 2014, JGRA, 119, 2269
Janches, D., Mathews, J., Meisel, D., Getman, V., & Zhou, Q. 2000a, Icar, 143, 347
Janches, D., Mathews, J., Meisel, D., & Zhou, Q. 2000b, Icar, 145, 53
Janches, D., Nolan, M., Meisel, D., et al. 2003, JGR, 108, 1222
Janches, D., Nolan, M., & Sulzer, M. 2004, ACP, 4, 621
Janches, D., & ReVelle, D. 2005, JGRE, 110, A08307
Jones, J., & Brown, P. 1993, MNRAS, 265, 524
Jones, W. 1997, MNRAS, 288, 995
Kero, J., Szasz, C., Nakamura, T., et al. 2012, MNRAS, 425, 135
Kleyn, A. W., Hubers, M. M., & Los, J. 1978, CP, 34, 55
Langowski, M., von Savigny, C., Burrows, J. P., et al. 2014, ACPD, 14, 1971
Love, S., & Brownlee, D. E. 1993, Sci, 262, 550
Marsh, D., Janches, D., Plane, J., & Feng, W. 2013, JGRD, 118, 11442
Mathews, J. D., Meisel, D. D., Hunter, K. P., Getman, V. S., & Zhou, Q. 1997, Icar, 126, 157
Moutinho, A. M. C., Baede, A. P. M., & Los, J. 1971, Phy, 51, 432
Nesvorný, D., Janches, D., Vokrouhlický, D., et al. 2011a, ApJ, 743, 129
Nesvorný, D., Jenniskens, P., Levison, H. F., et al. 2010, ApJ, 713, 816
Nesvorný, D., Vokrouhlický, D., Pokorný, P., & Janches, D. 2011b, ApJ, 743, 37
Pifko, S., Janches, D., Close, S., et al. 2013, Icar, 223, 444
Plane, J. 2003, Chem. Rev., 103, 4963
Plane, J. M. C. 1991, IRPC, 10, 55
Plane, J. M. C. 2012, ChSRv, 41, 6507
Pokorný, P., Vokrouhlický, D., Nesvorný, D., Campbell-Brown, M., & Brown, P. 2014, ApJ, 789, 25
Schlegel, H. B., Iyengar, S. S., Li, X., et al. 2002, JChPh, 117, 8694
Sekanina, Z. 1976, Icar, 27, 265
Smith, I. 1980, Kinetics and Dynamics of Elementary Gas Reactions (London: Butterworths)
Sparks, J. J., & Janches, D. 2009a, GeoRL, 36, 17101
Sparks, J. J., & Janches, D. 2009b, GeoRL, 36, 12105
Sparks, J. J., Janches, D., Nicolls, M. J., & Heinselman, C. J. 2009, JASTP, 71, 644
Taylor, A. 1997, AdSpR, 20, 1505
Taylor, A., & Elford, W. 1998, EP&S, 50, 569
Vondrak, T., Plane, J. M. C., Broadley, S., & Janches, D. 2008, ACP, 8, 7015
Webster, A. R., Brown, P. G., Jones, J., Ellis, K. J., & Campbell-Brown, M. 2004, ACPD, 4, 1181
Weiss, A. A., & Smith, J. W. 1960, MNRAS, 121, 5
Weryk, R. J., & Brown, P. G. 2013, P&SS, 81, 32
Zook, H. A. 1975, LPSC, 6, 898